The histone lysine methyltransferase Ezh2 is required for maintenance of the intestine integrity and for caudal fin regeneration in zebrafish

Barbara Dupret, Pamela Völkel, Constance Vennin, Robert-Alain Toillon, Xuefen Le Bourhis, Pierre-Olivier Angrand

▶ **To cite this version:**

Barbara Dupret, Pamela Völkel, Constance Vennin, Robert-Alain Toillon, Xuefen Le Bourhis, et al.. The histone lysine methyltransferase Ezh2 is required for maintenance of the intestine integrity and for caudal fin regeneration in zebrafish. Biochimica et Biophysica Acta - Gene Regulatory Mechanisms , 2017, 1860 (10), pp.1079-1093. 10.1016/j.bbagrm.2017.08.011 . hal-04449216

HAL Id: hal-04449216
https://hal.science/hal-04449216v1

Submitted on 9 Feb 2024

HAL is a multi-disciplinary open access archive for the deposit and dissemination of scientific research documents, whether they are published or not. The documents may come from teaching and research institutions in France or abroad, or from public or private research centers.

L'archive ouverte pluridisciplinaire **HAL**, est destinée au dépôt et à la diffusion de documents scientifiques de niveau recherche, publiés ou non, émanant des établissements d'enseignement et de recherche français ou étrangers, des laboratoires publics ou privés.

The histone lysine methyltransferase Ezh2 is required for maintenance of the intestine integrity and for caudal fin regeneration in zebrafish

Barbara Dupret[1¶], Pamela Völkel[1,2¶], Constance Vennin[1,3], Robert-Alain Toillon[1], Xuefen Le Bourhis[1] and Pierre-Olivier Angrand[1*]

[1] Cell Plasticity & Cancer, Inserm U908 / University of Lille, Lille, France

[2] CNRS, Lille, France

[3] SIRIC ONCOLille, Lille, France

* Corresponding author

Cell Plasticity & Cancer, Inserm U908 / University of Lille, Bâtiment SN3, Cité Scientifique, F-59655 Villeneuve d'Ascq, France.

Tel.: + 33 3 20 33 62 22

E-mail: pierre-olivier.angrand@univ-lille1.fr

[¶] These authors contributed equally to this work

GRAPHICAL ABSTRACT

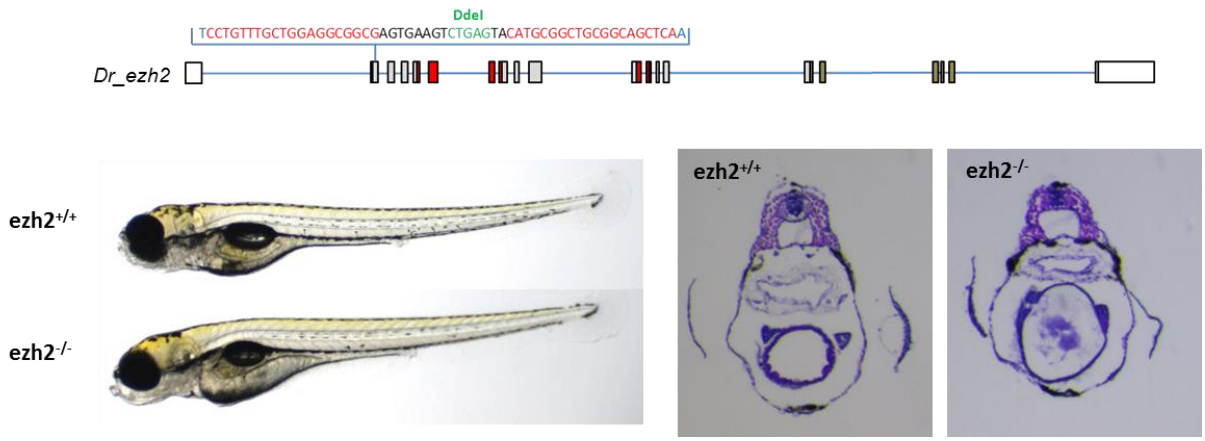

HIGHLIGHTS

- Zebrafish *ezh2*$^{-/-}$ mutants gastrulate properly and present a normal body plan.
- Zebrafish *ezh2*$^{-/-}$ mutants die at 12 dpf with defects of the intestine wall.
- Ezh2 function is required for intestine and exocrine pancreas maintenance.
- Loss of Ezh2 function is responsible for a strong increase in apoptosis.
- Ezh2 is required for regeneration of the larval caudal spinal cord after transection.

ABSTRACT

The histone lysine methyltransferase EZH2, as part of the Polycomb Repressive Complex 2 (PRC2), mediates H3K27me3 methylation which is involved in gene expression program repression. Through its action, EZH2 controls cell-fate decisions during the development and the differentiation processes. Here, we report the generation and the characterization of an *ezh2*-deficient zebrafish line. In contrast to its essential role in mouse early development, loss of *ezh2* function does not affect zebrafish gastrulation. *Ezh2* zebrafish mutants present a normal body plan but die at around 12 dpf with defects in the intestine wall, due to enhanced cell death. Thus, *ezh2*-deficient zebrafish can initiate differentiation toward the different developmental lineages but fail to maintain the intestinal homeostasis. Expression studies revealed that *ezh2* mRNAs are maternally deposited. Then, *ezh2* is ubiquitously expressed in the anterior part of the embryos at 24 hpf, but its expression becomes restricted to specific regions at later developmental stages. Pharmacological inhibition of Ezh2 showed that maternal Ezh2 products contribute to early development but are dispensable to body plan formation. In addition, *ezh2*-deficient mutants fail to properly regenerate their spinal cord after caudal fin transection suggesting that Ezh2 and H3K27me3 methylation might also be involved in the process of regeneration in zebrafish.

KEYWORDS: Zebrafish - TALEN - Polycomb repression – Ezh2 – GSK126.

LIST OF ABBREVIATIONS: bp: base pair; dpf: days post fertilization; dpa: days post amputation; ezh2: enhancer of zeste homolog 2 (polycomb repressive complex 2 subunit); hpf: hours post fertilization; gcga, glucagon a; ins: insulin; NMD: nonsense-mediated decay; nt: nucleotide; phox2bb: paired-like homeobox 2bb; PRC: Polycomb Repressive Complex; rnf2: ring finger protein 2; TALEN: transcription activator-like effector nuclease; try: trypsin.

1. INTRODUCTION

Polycomb-group (PcG) proteins are epigenetic repressors of transcriptional programs involved in the maintenance of cellular identity during development and differentiation [1- 3]. PcG proteins assemble into at least two well-characterized and biochemically distinct chromatin-modifying protein complexes that are termed Polycomb Repressive Complex 1 and 2 (PRC1 and PRC2). In the canonical pathway, PRC2 composed of the core proteins EZH2, EED and SUZ12 together with RBAP46/48 and other accessory subunits, initiates gene silencing by catalyzing di- and trimethylation of lysine 27 of histone H3 (H3K27me2/3) [4-8]. PRC1 is then recruited to the target regions by binding to H3K27me3 marks through the CBX component of PRC1 [9], and subsequently catalyzes the monoubiquitinylation of H2AK119 (H2AK119ub1) to maintain gene silencing [10-12].

Within the PCR2, EZH2 is a SET domain-containing protein harboring the histone methyltranferase activity, whereas EED and SUZ12 are involved in PRC2 stability and are necessary for EZH2 catalytic activity [13-15]. Genome-wide studies in mouse and human embryonic stem cells revealed that PRC2 and H3K27me3 marks are deposited at the promoters of numerous genes involved in cell differentiation, lineage specification and development, leading to the idea that EZH2 may be involved in the maintenance of the pluripotency of stem cells by keeping developmental genes repressed [9, 16-22]. Differentiation would then be associated with a relocation of PRC2, in turn responsible for the repression of the stem cell genes and enabling activation of gene expression programs specific to given developmental lineages. Indeed, the PRC2 components are essential for early mouse development and knock-out mutants for *Ezh2*, *Eed* and *Suz12* initiate but fail to complete gastrulation and die at around embryonic days 7 to 9 [14, 23, 24]. This death correlates with the alteration of lineage-specifying gene expression, a decrease in cell proliferation and an increase of apoptosis [14].

In human, recent cancer genome sequencing and expression studies reported that several genes encoding PRC2 subunits are mutated or have their expression altered in different cancer types [25, 26]. Furthermore, mutations in EZH2 were shown to cause the Weaver syndrome (OMIM:277590), a syndrome characterized by skeletal overgrowth, tall stature, a dysmorphic craniofacial appearance and variable intellectual disability [27-30].

The zebrafish model provides a unique tool to investigate gene function during development. The zebrafish (*Danio rerio*) is a widely used vertebrate model for studying development and morphogenesis. Owing to external fertilization and optical transparency of the embryos, early development of zebrafish can be easily monitored. Furthermore, the recent emergence of powerful genome-editing technologies, such as the Transcription Activator-Like Effector Nuclease (TALEN) and Clustered Regularly Interspaced Short Palindromic Repeats / CRISPR-associated System (CRISPR/Cas9) applied to zebrafish allows rapid gene function studies in this organism [31-36]. Using the TALEN technology, we generated here a heterozygous zebrafish line harboring an *ezh2* loss-of-function allele to investigate its role in development. We show that in contrast to what is observed in mice, *ezh2* zygotic expression is not required for gastrulation and tissue specification in zebrafish. However, homozygous mutants die at about 12 dpf with defects in the intestine wall, suggesting that zygotic *ezh2* expression is necessary for the maintenance of the integrity of the intestine at later developmental time points. Furthermore, we show that the ability of spinal cord regeneration at the caudal fin is also affected in homozygous mutant larvae.

2. MATERIALS AND METHODS

2.1. Zebrafish maintenance, embryo preparation and treatment. Zebrafish (TU strain) were maintained at 27.5°C in a 14/10h light/dark cycle. The evening before spawning, males and females were separated into individual tanks. Spontaneous spawning occurred when the light turned on and embryos or larvae were collected and staged according to Kimmel et al. [37]. The feeding of zebrafish larvae starts at 6 dpf for all experiments. The chorions were removed from embryos by the action of 1% pronase (Sigma) for 1 min. Zebrafish embryos or larvae were fixed overnight in 4% paraformaldehyde in PBS (phosphate-buffered saline, Invitrogen), dehydrated gradually to 100% methanol and kept at -20°C.

For caudal fin amputation, 6-month-old adult zebrafish were anesthetized with MS-222 (tricaine, ethyl 3-aminobenzoate methanesulphonate, 250 mg/L; Sigma-Aldrich) and approximately two-thirds of the fin was cut with a blade. After amputation, fish were placed in the aquarium at 27.5°C for fin regeneration. The blastemal starts to form at approximately 24 hours post amputation (hpa) and the amputated fins have been fully restored at around 20 days post amputation (dpa). Larval caudal fin transections were performed at 3 dpf within the pigment gap distal to the circulating blood after anesthesia, as described by Wilkinson et al. [38].

To inhibit Ezh2 activity, dechorionated embryos were exposed to 1 µM GSK126 (A11757, Adooq Bioscience) dissolved in DMSO or to an equivalent concentration of DMSO (0.01%, control) at the 1-2 cell stage, at 3 hpf or after larval caudal fin amputation.

2.2. Animal ethics statement. The zebrafish experiments described in this study were conducted according to the French and European Union guidelines for the handling of laboratory animals (Directive 2010/63/EU of the European Parliament and of the Council of 22 September 2010 on the protection of animals used for scientific purposes). The experimental procedures carried out on zebrafish were reviewed and approved by the local Ethics Committee of the Animal Care Facility of the University of Lille. At the end of the experiment, fish older than 8 dpf were humanely euthanized by immersion in an overdose of tricaine methane sulfonate (MS-222, 300 mg/L) for at least 10 minutes, whereas younger fish were immobilized by submersion in ice water (5 parts ice/1 part water, 0-4°C) for at least 1 hour to ensure death by hypoxia.

2.3. TALEN design and assembly. The *ezh2*

TALEN target site was selected using the online TAL Effector-Nucleotide Targeter tool (https://tale-nt.cac.cornell.edu/; [39]) in exon 2 with the following parameters: (i) spacer length of 14–17 bp, (ii) repeat array length of 16–18 bp, (iii) each binding site was anchored by a preceding T base in position ‘‘0’’ as has been shown to be optimal for naturally occurring TAL proteins [40, 41], (iv) presence of a restriction site (DdeI) within the spacer sequence for screening and genotyping purposes.

Ezh2-specific TALEN constructs were engineered using the TALEN Golden Gate assembly system described by Cermak et al., [42]. The TALEN expression backbones, pCS2TAL3DD and pCS2TAL3RR [31], and the plasmids providing repeat variable diresidues (RVD) [42] for Golden Gate Cloning were obtained from Addgene.

2.4. mRNA injection into zebrafish embryos. Capped mRNAs were synthetized using the SP6 mMESSAGE mMACHINE kit (Ambion) from linearized plasmid templates. mRNAs (50-100 pg) were injected into 1-cell zebrafish embryos using a FemtoJet microinjector (Eppendorf).

2.5 Genotype analyses. Three-days-old embryos or pieces of caudal fin were incubated in 20 µL PCR extraction buffer (10 mM Tris-HCl pH8.0, 2 mM EDTA, 0.2% Triton X-100, 100 µg/mL Proteinase K) and placed at 50°C for 4 hours prior proteinase K inactivation at 95°C for 5 min. Genotype analysis was performed by PCR on 2.5 µL of samples using the primer set TAL_ezh2_5’_S21Ac (GGTATGGTTGTTGCAGTTCACAGAC) and TAL_ezh2_3’_S21Ac (AACACCAAACTCTACACAAGCAGCA) followed by PCR product digestion with the DdeI restriction enzyme. Sequence determination (GATC-Biotech, Germany) was performed after cloning of the PCR products into pCR-XL-TOPO (Invitrogen) according to the manufacturer’s instructions.

To achieve genotyping on paraformaldehyde-fixed embryos and larvae, DNA was extracted using sodium hydroxide and Tris [43]. Briefly, single embryos were placed into microcentrifuge tubes containing 20 µL 50 mM NaOH and heated 20 min at 95°C. The tubes were then cooled to 4°C and 2 µL of 1 M Tris-HCl, pH7.4 was added to neutralize the basic solution. Genotype analysis was performed on 2.5 µL of samples by PCR-DdeI digestion, as described above.

2.6. Alcian blue staining. Alcian blue staining was performed as previously described [44]. Zebrafish larvae were fixed 2 hours at room temperature in 4% paraformaldehyde and dehydrated 10 min in 50% ethanol. Cartilages were stained in 0.02% Alcian blue (Sigma Aldrich), 60 mM $MgCl_2$, 70% ethanol, overnight at room temperature. Pigments were bleached by a 2-hours incubation in water containing 1% KOH, 3% H_2O_2. Larvae were then digested with 0.05% trypsin (Sigma Aldrich) until tissue disappeared (around 4 hours) before storage in 70% glycerol. After imaging with a Leica MZ125 stereomicroscope equipped with a Leica DFC295 digital camera, DNA was extracted using sodium hydroxide and Tris for genotyping purposes.

2.7. Whole-mount immunohistochemistry. Zebrafish embryos were fixed 2 hours at room temperature in 4% paraformaldehyde, followed by dehydration and storage overnight in methanol at -20°C. Embryos were then permeabilized in PBS containing 0.1% Tween20, 10 µg/mL proteinase K and blocked in PBS containing 0.1% Tween20 and 2% sheep serum.
For muscle development studies, the primary antibody used was a mouse anti-MF20 (1:20; Developmental Studies Hybridoma Bank, developed under the auspices of the NICHD and maintained by The University of Iowa, Department of Biology, Iowa City, IA 52242) and the secondary antibody was a peroxidase conjugated AffiniPure goat anti-mouse (1:500; 115-035-003, Jackson ImmunoResearch). The embryos were imaged using a Leica MZ125 stereomicroscope equipped with a Leica DFC295 digital camera. For H3K27me3 analyses, the primary antibody used was a rabbit anti-H3K27me3 (1:750; 07-449, Millipore) and the secondary antibody was an Alexafluor 546 conjugated goat anti-rabbit antibody (1:5,000; A11035, Invitrogen). The embryos were then imaged using a Leica MZ10F stereomicroscope equipped with a Leica DFC3000G digital camera. After imaging, DNA was extracted using sodium hydroxide and Tris and embryos were genotyped.

2.8. Oil red-O staining. Zebrafish larvae were fixed in 4 % paraformaldehyde overnight at 4°C and their pigments bleached by 2-hours incubation in a solution containing 1% KOH and 3% H_2O_2. Larvae were washed five times in PBS and stained with oil red-O (Hamiya Biomedical Company) for 15 min. Stained larvae were washed with PBS, stored in 70% glycerol and imaged on a bright-field dissecting microscope (Leica MZ125) equipped with a Leica DFC295

digital camera. After imaging, DNA was extracted using sodium hydroxide and Tris for genotyping analyses.

2.9. Histological analyses. For histological analyses, tail biopsies were used for genotyping before paraformaldehyde fixation of the larvae. Larvae were embedded in paraffin and cut into 5 µm-thick sections. These were mounted on sylanated glass slides, deparaffinated, rehydrated and stained with hematoxylin and eosin for histological analysis.
Immunostainings on zebrafish sections were done to visualize actin using a rabbit anti-actin primary antibody (1:50; A2066, Sigma) and a horseradish peroxidase conjugated anti-rabbit IgG secondary antibody (1:500; 711-035-152, Jackson ImmunoResearch) and counterstained with hematoxylin (RAL Diagnostic) for nuclear staining. F-actin was visualized by Alexa fluor 594 conjugated phalloidin (1:100; A12381, Thermofisher) staining and nuclear counterstaining done with 1 mM Hoechst 33258 (861405, Sigma). Image acquisition was performed using a Nikon Eclipse Ti microscope equipped with a Nikon DXM1200C digital camera.

2.10. TUNEL assay. TUNEL assays were performed using the In Situ Cell Death Detection Kit (Roche, 11 684 817 910), according to the manufacturer's instructions. Briefly, larvae were embedded in paraffin and cut into 5 µm-thick sections. These were mounted on sylanated glass slides, deparaffinated, rehydrated and digested 10 min at room temperature with 3 U/mL DNase I in 50 mM Tris-HCl pH7.5, 10 mM $MgCl_2$, 1 mg/mL BSA. The TUNEL Reaction Mixture was added to slides, incubated 1 hour at 37°C, rinsed 3 times with PBS before addition of the Converter-POD for 30 min at 37°C. Samples were rinsed 3 times with PBS, incubated 45 min at room temperature in presence of the DAB substrate, washed 3 times with PBS, dehydrated and mounted under glass coverslips. The images were acquired using a Nikon Eclipse Ti microscope equipped with a Nikon DXM1200C digital camera.

2.11. Whole-mount in situ hybridization. For *ezh2*, *ins* and *gcga*, antisense RNA probes were synthesized with the DIG RNA Labeling Kit (SP6/T7) (Roche, 11175025910), following the manufacturer's instructions from 1 µg of linearized plasmid DNA. The cDNA clone MGC:152758 IMAGE:2639510 purchased at imaGenes GmbH (Berlin) was used for *ezh2* probes, whereas *ins* and *gcga* cDNA containing vectors were a gift from Dr Julien Bricambert and Pr Amar Abderrahmani (CNRS UMR 8099, EGID). *try* and *phox2bb* probes were generated

using RT-PCR from total mRNA extracted from zebrafish larvae at 5 dpf using the RNeasy Mini Kit (Qiagen), following the manufacturer's protocol. After Reverse Transcription (Superscript III, Invitrogen), cDNAs were amplified by PCR using the probe specific primers, coupled to the T7 sequence for forward primers and the SP6 sequence for reverse primers. DIG labelled Antisense-RNA probes have been synthetized using the DIG RNA Labeling Kit (SP6) (Roche), following the manufacturer's instructions.

The primers used for probe generation were:

ISH_try_F:	TAATACGACTCACTATAGGGTGCTCACTGCTACAAGTCCCGT
ISH_try_R:	GATTTAGGTGACACTATAGCCCGAGCTTAGTTGGAGTTCATGGT
ISH_phox2bb_F:	TAATACGACTCACTATAGGGGGGCCTAACCCGAACCCTACCTC
ISH_phox2bb_R:	GATTTAGGTGACACTATAGGAGCGCACATCGCAGTCTATCGG

In situ hybridization was performed as described by Thisse and Thisse [45]. Briefly, the fixed embryos were rehydrated and permeabilized with 10 µg/mL proteinase K for 30 sec (1 to 2-cell embryos), 10 min (24 hpf embryos) or 30 min (48 to 120 hpf embryos) at room temperature. Ten to 50 embryos from each time point were hybridized with digoxigenin-labeled antisense RNA probes at 70°C. After extensive washing, the probes were detected with anti-digoxigenin-AP Fab fragment (Roche Diagnostics, 1093274, diluted at 1:10,000), followed by staining with BCIP/NBT (5-bromo-4-chloro-3-indolyl-phosphate/nitro blue tetrazolium) alkaline phosphate substrate. The embryos were imaged using a Leica MZ125 stereomicroscope equipped with a Leica DFC295 digital camera.

Regenerating fins from adult fish or fin amputated larvae were fixed in 4% paraformaldehyde overnight, then rehydrated and permeabilized with 10 µg/mL proteinase K for 10 min (5 dpf larvae) or 40 min (adult fish) before whole-mount *in situ* hybridization and imaging.

To visualize *ezh2* mRNA signals in the eye, the digoxigenin-labeled and hybridized antisense RNA probes were detected using tyramide signal amplification (TSA)-Cy5 reagent (Roche) according to Brend and Holley [46]. Larvae were then embedded in paraffin, cut into 5-µm-thick sections and the eye sections were imaged using a Nikon Eclipse Ti microscope equipped with a Nikon DXM1200C digital camera.

2.12. Histone extraction and western blot analysis. Histone extracts were prepared by lysis of 5 to 10 embryos per tube in PBS containing 0.5% Triton X-100, 2mM phenyl-methylsulfonyl fluorid (PMSF), 0.02% NaN_3, 10 min on ice. After centrifugation, the pellet was resuspended

in 0.2 N HCl and core histones extracted overnight at 4°C while rocking. Samples were centrifuged and the supernatant containing the histones was stored at -20°C.

For Western blotting, protein samples in SDS loading buffer were electrophoresed on 4-12% Bis-Tris gels (NuPAGE, Invitrogen) and transferred to nitrocellulose membranes using the iBlot® Dry Blotting System (Invitrogen). Efficiency of the transfer is verified by immersing the blotted membrane into a Ponceau S staining Solution (0.1% Ponceau S in 5% acetic acid, Sigma). The membranes were then destained and blocked in 5% milk powder in PBS-T (1x PBS with 0.1% Tween20) for 1 hour at room temperature, incubated for the same time with the primary antibody in PBS-T, and washed three times 10 min in PBS-T. The membranes were then incubated with the peroxidase-conjugated secondary antibody in PBS-T for 1 hour and afterward washed three times 10 min in PBS-T. The signal was detected using a chemiluminescence substrate (Western Lightning Ultra, PerkinElmer) with a Luminescent Image Analyzer (LAS-4000, Fujifilm).

Primary antibodies used were mouse anti-H3K27me3 (1:1,000; ab6002, Abcam) and rabbit anti-H3 (1:5,000; ab1791, Abcam). The secondary antibodies were peroxidase conjugated anti-mouse antibody (1:10,000; 115-035-003, Jackson ImmunoResearch) and peroxidase conjugated anti-rabbit antibody (1:10,000; 711-035-152, Jackson ImmunoResearch).

2.13. RNA extraction and RT-PCR. Total RNA was isolated from 2 hpf, 3 dpf, 5 dpf and 9 dpf wild-type and mutant embryos or larvae using Trizol. cDNA was synthesized using Superscript III (18080-044, Invitrogen). To recover *ezh2* transcripts, a forward primer in Exon 1 (GAGGTGAAAGGACCCTCTACC) and a reverse primer in Exon 3 (CTCAGTTTCCATTCCTGATTTAAG) were used, whereas *β-actin* primers were already published (b-actinF: CGTGACATCAAGGAGAAGCT and b-actinR: ATCCACATCTGCTGGAAGGT) [47].

3. RESULTS

3.1. TALEN-mediated ezh2 inactivation in zebrafish. To gain insights into the function of *ezh2* in zebrafish development, we generated *ezh2* loss-of-function mutants using the transcription activator-like effector (TALE) nuclease (TALEN)-based technology. TALENs consist in the fusion of the endonuclease domain of the restriction enzyme FokI to engineered sequence-specific DNA-binding domains from TALEs in order to target the nuclease activity to chosen genomic sequences. Once activated through dimerization, the FokI catalytic domain introduces a double strand DNA break which is repaired through the non-homologous end joining (NHEJ) pathway. This repairing process is error prone and may introduce insertion and/or deletion (*indel*) mutations. Among the resulting mutations, several will lead to shifts in the open reading frame, impairing the resulting protein sequence. TALENs were designed to target a region within the second exon of *ezh2* in order to introduce a frame shift upstream of all known Ezh2 conserved domains, including two SANT domains and the catalytic SET domain. In addition, the targeted region was chosen to contain a DdeI restriction site that could be used to screen for mutations and for genotyping purposes (**Figure 1A**). TALENs were assembled using the Golden Gate Cloning methodology [42] and *in vitro* transcribed mRNAs encoding each TALEN pair were injected into one-cell stage embryos. Genomic DNA was extracted from single embryos collected at 3 days after TALEN mRNA injection. PCR amplification of the targeted region, followed by DdeI digestion revealed the efficacy of the designed TALENs and the convenience of the diagnostic restriction site as a genotyping strategy (**Figure 1B**).

When analyzed by restriction of genomic DNA at 3 days after TALEN mRNA injection, the mutation rate at the *ezh2* locus was about 94% (17 of 18 injected embryos tested). Then, we raised TALENs-injected embryos to establish an adult F0 founder population. To evaluate the efficiency of germ line transmission of the mutations, individual F0 fish carrying mutations were crossed to wild-type TU partners to obtain F1 offspring. Genomic DNA was isolated from individual F1 embryos from each F0 fish and analyzed by DdeI restriction. Embryos from 3 of 14 individual F0 fish were heterozygous mutants, demonstrating successful germ line transmission of the mutations. One mutation causes a 22 bp net insertion (insertion of 27 nucleotides together with a deletion of 5 bp) leading to a frame shifting of the coding sequence and appearance of a premature stop codon (**Figure 1C**). This $ezh2^{+22}$ allele codes for

a predicted protein of 60 amino acids, lacking all conserved protein domains (**Figure 1D**, **Supplementary Figure S1**) and was selected to raise the mutant *ezh2*$^{+/-}$ zebrafish line used for further phenotypic studies after outcross to wild-type TU fish. Heterozygous *ezh2*$^{+/-}$ fish are viable, fertile and do not show any phenotype. Surprisingly, among siblings from heterozygous *ezh2*$^{+/-}$ crosses, homozygous *ezh2*$^{-/-}$ fish were identified till 12 dpf indicating that *ezh2* zygotic function is not required for zebrafish early development. Furthermore *ezh2*$^{-/-}$ mutant fish do not present gross morphological alterations (**Figure 2A**) and show a normal craniofacial cartilage and muscle development (**Figure 2B-C**). However, we could not identify *ezh2*$^{-/-}$ fish after 12 dpf suggesting that zygotic *ezh2* function is required for zebrafish development at this time point.

3.2. Ezh2 expression during zebrafish development. In order to study *ezh2* mRNA expression, embryos from heterozygous *ezh2*$^{+/-}$ crosses were subjected to whole-mount *in situ* hybridization (**Figure 3**). At the 2-cell stage, maternal *ezh2* mRNAs are detected in the embryo (**Figure 3A**). To investigate whether the maternally provided transcripts correspond to wild type and/or mutant products, RNAs were extracted, amplified by RT-PCR and the PCR products were subjected to DdeI digestion. **Figure 3B** shows that these maternal transcripts are mainly derived from the wild-type allele, but not from the mutant allele, suggesting that mutant *ezh2* transcripts are subjected to nonsense-mediated decay (NMD) in the zebrafish female germline. *In situ* hybridization experiments revealed that *ezh2* is ubiquitously expressed in the anterior part of wild-type embryos at 24 hpf, but its expression becomes restricted to specific regions such as the pectoral fin buds, the optic tectum, the mid-hindbrain region, the branchial arches, the eyes and the intestine, at later developmental stages (**Figure 3C-D, Supplementary Figure S2A**). This restricted *ezh2* expression correlates with a decrease of total *ezh2* mRNA abundance assessed by RT-PCR (**Supplementary Figure S2B**).

In mutant embryos, only a weak hybridization signal could be detected by *in situ* hybridization **(Figure 3C-D**). This residual *ezh2* expression is found in the same restricted regions as found in wild-type embryos, suggesting that these transcripts do not derive from maternally deposited products. Indeed, studies of *ezh2* mRNAs found in mutant embryos by RT-PCR, followed by DdeI cleavage and sequencing, show that these transcripts contain the +22 nt net insertion and consequently arise from the transcription of the mutant allele (**Supplementary Figure S2C-D**). This also indicates that mutant *ezh2* mRNAs escape, at least in part, to NMD

regulation in *ezh2*$^{-/-}$ embryos. Altogether, our results demonstrate that maternal wild-type transcripts are present at very early developmental stages, but are not maintained at later stages. Furthermore, *ezh2* zygotic expression is ubiquitous and relatively high at 24 hpf, but becomes restricted to a limited number of tissues at later developmental stages.

3.3. Ezh2 mutant fish die at around 12 dpf with intestine defects. To investigate in more details why *ezh2*$^{-/-}$ embryos die at 12 dpf, zebrafish larvae from *ezh2*$^{+/-}$ crosses were stained with the neutral lipid dye oil red-O in order to better visualize the digestive organs. At 9 dpf, this lipid staining reveals marked differences between *ezh2*$^{-/-}$ and their *ezh2*$^{+/+}$ counterparts (**Figure 4A**). In particular, the liver shows a stronger coloration in mutant fish, suggesting that the lipid composition might change in absence of *ezh2* function. More strikingly, oil red-O staining points out differences in the structure of the intestine. In mutant *ezh2*$^{-/-}$ fish, the intestine epithelium looks finer than in wild-type fish. This observation was confirmed by the analysis of histological sections of larvae at 9 dpf (**Figure 4B**). The intestine wall of *ezh2*$^{-/-}$ mutants is strongly reduced and lacks folds in the intestine bulb. In contrast, the architecture of more proximal and distal parts of the digestive tract does not present such defects in the mutants at 9 dpf and 11 dpf (**Supplementary Figure S3A**). Interestingly, at 5 dpf, when the digestive tract achieves its formation and compartmentalization [48], the structure of the intestine wall in all regions is similar in both *ezh2*$^{-/-}$ and *ezh2*$^{+/+}$ siblings (**Figure 4B, Supplementary Figure S3B**). This indicates that the development of the intestine is normal, but its structure cannot be maintained in *ezh2*$^{-/-}$ mutant fish, then leading to their death at 12 dpf. To determine whether the absence of maintenance of the intestine structure results from an enhanced cell death, we performed a terminal deoxynucleotidyl transferase-mediated dUTP nick end labeling (TUNEL) assay for detecting DNA fragmentation generated during apoptosis, on intestine sections at 9 dpf. As shown on Figure 4C, the altered intestine structures in *ezh2*$^{-/-}$ mutant are strongly stained by the TUNEL assay, indicating that the absence of maintenance of the intestine integrity is due to a massive increase in apoptosis.

3.4. Ectopic expression of phox2bb in ezh2 mutants. Since the development of the enteric nervous system is critical for normal functioning of the digestive system, we performed *in situ* hybridizations to detect *phox2bb* expression. Phox2bb is a transcription factor required for the specification of enteric neural crest fate [49] and its expression is used to monitor the

localization of the enteric progenitors. Our study reveals that the organization of the enteric neural crest cells along the rostral-caudal axis of the gut tube is similar in wild-type and *ezh2* mutant fish at 5 dpf (**Figure 5A**). However, we could detect striking differences in *phox2bb* expression in the eyes (**Figure 5B-C**). *Phox2bb* expression is not detected by *in situ* hybridization in the eyes of wild-type larvae whereas *ezh2* positive cells can be visualized in the retina. In contrast, *ezh2*$^{-/-}$ siblings which do not express the *ezh2* transcripts, ectopically express *phox2bb* in the eye. This observation suggests that Ezh2 may negatively control *phox2bb* expression in the eye.

To further investigate the expression of *ezh2* in the eye, *in situ* hybridization experiments on wild-type larvae at 9 dpf using digoxygenin-labeled *ezh2* riboprobes and tyramide signal amplification (TSA)-Cy5 reagent [50] were performed prior sections of the eyes. This approach revealed that *ezh2* is expressed in the cornea and in all the layers of the retina, but not in the inner plexiform, the outer plexiform, and the retinal pigmented epithelium (**Figure 5D**). However, in spite of the loss of the Ezh2 product and ectopic expression of *phox2bb*, observed at 5 dpf, we could not identify histological alteration in the eyes of *ezh2*$^{-/-}$ fish, later at 9 dpf, when compared to wild-type siblings (**Figure 5E**).

3.5 Loss of ezh2 function affects the development of the exocrine pancreas. Because *ezh2*$^{-/-}$ mutants show defects in digestive organs including the intestine and the liver, we investigated the development of the pancreas (**Figure 6**). *In situ* hybridization experiments at 5 dpf with probes for the markers of the endocrine pancreas *ins* and *gcga*, revealing β- and α-cells respectively, do not highlight differences between *ezh2*$^{-/-}$ and *ezh2*$^{+/+}$ siblings. In contrast, *in situ* hybridization for *try*, a terminal differentiation marker for the exocrine pancreas, revealed that this organ is less developed in the *ezh2*$^{-/-}$ mutant fish (**Figure 6A**, **Supplementary Figure S4**).

To determine whether the reduced size of the exocrine pancreas is an early or late event, we assayed for *try* expression at 3 dpf. **Figure 6B** shows that at this stage, the exocrine pancreas development is similar in *ezh2*$^{-/-}$ and *ezh2*$^{+/+}$ siblings. This indicates that, as for the intestine development, the development of the exocrine pancreas in fish lacking embryonic *ezh2* expression is normally formed at early stages but its proper maintenance is affected at later developmental stages.

3.6. Impaired H3K27me3 methylation in ezh2 mutant zebrafish. Since Ezh2 trimethylates lysine 27 of histone H3 (H3K27), we evaluated the trimethylation status of histone H3 at lysine 27 in *ezh2*$^{-/-}$ mutant fish. Total histones were extracted from mutant and wild-type siblings at 9 and 12 dpf and trimethylation of lysine 27 of histone H3 was analyzed by western blot using a specific anti-H3K27me3 antibody. **Figure 7A** shows that global levels of trimethylated lysine 27 of histone H3 are severely decreased but not abolished, in *ezh2*$^{-/-}$ mutants at both developmental time points. Interestingly, heterozygous *ezh2*$^{+/-}$ fish show intermediated levels of global H3K27me3 methylation (**Figure 7B**), indicating that *ezh2* haploinsufficiency is responsible for a decrease in H3K27me3 methylation without affecting the phenotype, whereas homozygous loss of *ezh2* does not fully abolish H3K27me3 levels but leads to cell death and loss of maintenance of the intestine structures. Whole-mount *in situ* immunodetection of H3K27me3 at 24 hpf does not show staining differences between *ezh2*$^{+/+}$ and *ezh2*$^{-/-}$ siblings suggesting that Ezh2 maternal products and/or Ezh1 are the main factors involved in H3K27me3 methylation at this stage (**Figure 7C**). In contrast, *in situ* immunostaining for H3K27me3 at 4 dpf reveals a reduction of global levels of this epigenetic mark in *ezh2*$^{-/-}$ mutants. Moreover, this decrease affects all tissues of the organism, rather than specific tissues (**Figure 7C**).

3.7. Pharmacological inhibition of Ezh2 alters zebrafish development. Maternal *ezh2* transcripts are detected at the embryonic 1-2 cell stage. In order to investigate the role of maternally deposited Ezh2 products in early zebrafish development, we used a pharmacological approach to inhibit Ezh2 activity at early developmental stages. Dechorionated embryos were exposed to the EZH2 specific inhibitor GSK126 [51] at 3 hpf. The GSK126 was chosen to inhibit Ezh2 activity because this drug acts *in vivo* and is 150-fold selective for EZH2 over EZH1 and more than 1,000-fold selective for EZH2 over a range of other methyltransferases [52]. Since zebrafish embryo and larvae rapidly absorb low molecular weight compounds, diluted in the surrounding media, through skin and gills the treatment concentrations used were the same as described for applications in cells in culture [51]. Morphological abnormalities were first detected at 24 hpf with 1 µM GSK126 (**Figure 8A-B**). At 96 hpf, phenotypic aberrations include cardiac edemas, absence of pectoral fins (**Figure 8B**), as well as a decrease in eye size (**Figure 8C**). Further investigations revealed that the loss of pectoral fins, as well as the reduced size of the eyes of the treated embryos reflects a

developmental delay rather than a developmental alteration, since pectoral fins appear later. None of these phenotypes, such as the appearance of cardiac edemas and developmental delays, were observed in *ezh2*$^{-/-}$ mutants indicating that the inhibition of Ezh2 activity at 3hpf more severely affects zebrafish development. To determine whether GSK126 exposure affected total H3K27me3 methylation levels, dechorionated embryos cultured from 3 hpf to 96 hpf in presence of 1 µM GSK126, were analyzed by Western blotting using a specific anti-H3K27me3 antibody. We show that H3K27me3 relative levels were decreased by about 60% in treated embryos (**Figure 8D**). The whole-mount *in situ* immunodetection of H3K27me3 methylation shows that the decrease in H3K27me3 levels is rather global than limited to specific organs (**Figure 8E**). The remaining H3K27me3 levels are probably due to the fact that GSK126 blocks *de novo* Ezh2-mediated methylation, but do not affect H3K27me3 marks implemented before the drug exposure at 3 hpf. A similar experiment was conducted by applying 1 µM GSK126 on embryos at the 1-2 cell stage. In these conditions, gastrulation and the establishment of the body plan is seemingly normal, but the GSK126 treatment also induces cardiac edemas and developmental delays (**Supplementary Figure S5A**), as observed when the treatment is applied at 3 hpf, but not found in *ezh2*$^{-/-}$ mutants. H3K27me3 relative levels were deceased by about 35% in treated embryos (**Supplementary Figure S5B**).
Although the loss of H3K27me3 is not complete, inhibiting Ezh2 activity at the 1-2 cell stage or at 3 hpf elicits stronger developmental defects than the loss of zygotic Ezh2 activity underlying a role of the maternal Ezh2 products at early developmental stages. However, loss of maternal Ezh2 activity does not dramatically affect the establishment of the zebrafish body plan.

3.8. Ezh2 function is involved in caudal fin regeneration. Upon amputation, the zebrafish caudal fin fully regenerates in about 20 days. This regeneration process involves various cellular events such as wound closure, dedifferentiation, mesenchymal proliferation, blastema formation and outgrowth, actinotrichia formation, apical blastema maintenance, progressive redifferentiation and morphogenesis [53]. Moreover, a role of H3K27 methylation in caudal fin regeneration has been demonstrated [54]. *In situ* hybridization revealed that *ezh2* is expressed in the growing blastema of regenerating fins at 4 days post-amputation in adult zebrafish whereas the sense probe lacked any discernable signal (**Supplementary Figure S6**).

Since caudal fins of larvae also regenerate after amputation by a mechanism highly similar to that used by adult fish [55, 56], and because *ezh2*$^{-/-}$ adult fish are not viable preventing the study of the role of *ezh2* in caudal fin regeneration at this stage, we focused our attention on larval caudal fin regeneration. The tip of the caudal fin was transected at 3 dpf within the pigment gap distal to the circulating blood. This fin clip procedure induces blastema formation at the site of amputation followed by caudal fin regeneration and normal development of the embryo ([38]; **Figure 9**). Using *in situ* hybridization, we showed that *ezh2* expression is detected in larval caudal fin after amputation (**Figure 9A**). To investigate whether Ezh2 function is required for caudal spinal cord regeneration, larvae were subjected to caudal fin amputation at 3 dpf and the regeneration process was studied in presence of the Ezh2-specific inhibitor GSK126 (**Figure 9B**). In presence of 1 µM GSK126, regeneration of the fin fold and of the spinal cord is severely impaired, compared to control DMSO treated embryos. Similarly, the spinal cord of *ezh2*$^{-/-}$ larvae also fails to regenerate properly after transection, when compared to wild-type siblings (**Figure 9C**). Altogether, our results indicate that *ezh2* is expressed in the regenerating caudal fin after amputation and suggest that Ezh2 function is required for larval caudal spinal cord regeneration.

4. DISCUSSION

In the past decade, an increasing amount of data underlined the fundamental role of epigenetic modifications in controlling the activity of regulatory genes involved in development, lineage specification, differentiation and tissue renewal. In the present study, we examine the role of Ezh2 in zebrafish development. Ezh2 catalyzes the trimethylation of lysine 27 of histone H3 (H3K27me3), a post-translational modification that has been widely implicated in epigenetic suppression of gene expression.

To address the question of the function of Ezh2, we generated an *ezh2* loss-of-function allele in zebrafish using the TALEN technology. A zebrafish line harboring a 22 bp net insertion (insertion of 27 nucleotides associated with a deletion of 5 bp) within the *ezh2* gene, leading to a frame shift in the coding sequence and encoding a predicted protein of 60 amino acids, lacking all of the essential conserved protein domains, has been generated. The heterozygous *ezh2*$^{+/-}$ fish are viable, fertile, and do not show any obvious phenotype.

Surprisingly, and in total contrast to what was observed in mice where *Ezh2* loss-of-function results in lethality at gastrulation [24], homozygous *ezh2*$^{-/-}$ zebrafish mutants gastrulate properly and develop normally. However, at 9 dpf, the *ezh2*$^{-/-}$ mutant presents a striking alteration of the intestine wall, presumably responsible for the death of the *ezh2*$^{-/-}$ fish. Interestingly, at 5 dpf the intestine of *ezh2*$^{-/-}$ mutants is normal, indicating that this organ develops properly in absence of zygotic Ezh2 function, but that the maintenance of its structure requires Ezh2 action. The defects in the maintenance of the integrity of the intestine are due to enhanced cell death rather than to an arrest of development, as a TUNEL assay shows a massive increase of apoptosis in *ezh2* loss-of-function mutants. Remarkably, the structure of the intestine bulb is severely impaired in *ezh2* mutants at 9 dpf whereas the wall of the mid-intestine of *ezh2*$^{-/-}$ and wild-type siblings remains similar. Since the cell proliferation rate is higher in the intestine bulb than in the mid-intestine [57], our data also establish a link between Ezh2 function and intestinal cell renewal.

Zebrafish *ezh2*$^{-/-}$ mutants present alterations of the intestine and this phenotype differs to what has been found in mice. Indeed, using a Cre-mediated conditional knock-out approach, Koppens et al. [58] generated mice lacking Ezh2 activity in the intestine. These mutants present a reduction of H3K27me3 marks in the intestine but this does not result in an overt adverse phenotype, since the intestines lacking Ezh2 function are morphologically similar to

controls and cell proliferation and differentiation are not affected. Moreover, no difference can be observed between mice lacking Ezh2 function in the intestines and control mice [58]. This may suggest that Ezh2 contributes differently to the maintenance of the structure of the intestine in mice and in zebrafish.

Different mutations, including *sst*^{m311} (*straight shot*), *nor*^{m264} (*no relief*), *pie*^{m497} (*piebold*) or *polr3b*^{m74} (*polr3b*, *slim jim*), have been reported to be responsible for the intestine degeneration in zebrafish [59]. Moreover, it has also been shown that these mutations are responsible for alterations in the exocrine pancreas development [59]. Similarly, *ezh2*$^{-/-}$ mutants present defects in the development of the exocrine pancreas in addition to a striking intestinal phenotype. Indeed, the development of the exocrine pancreas, as judged by the expression of the terminal differentiation marker *try*, is impaired in *ezh2* deficient fish at 5 dpf. However, as for the intestine, the development of the exocrine pancreas in *ezh2*$^{-/-}$ mutants is normally formed at early stages (3 dpf). This indicates that zygotic *ezh2* expression is not required for exocrine pancreas implementation whereas Ezh2 in necessary to properly maintain the development of this organ at later stages.

The analyses of mRNA expression profile of *ezh2* in zebrafish showed that maternal transcripts are detected in the embryo at the 2-cell stage. At 24 hpf, the *ezh2* mRNA is ubiquitously expressed, whereas its expression becomes restricted to defined regions such as the pectoral fin buds, the optic tectum, the mid-hindbrain region, the branchial arches, the eyes and the intestine during later development, as recently shown by San et al. [60]. This observation parallels the experiments performed in mouse showing that murine *Ezh2* is ubiquitously expressed throughout early embryogenesis, while in later embryonic development, *Ezh2* expression tends to be restricted to specific sites within the central and peripheral nervous system and to the major sites of fetal hematopoiesis, as well as in the intestine, the testis, the placenta and the muscles [61, 62].

The presence of *ezh2* mRNAs in the early zebrafish embryo suggests that maternally deposited *ezh2* products may be involved in early development. Since maternal contribution takes place till the 2-cell stage in mice whereas in zebrafish maternal contribution could be maintained until at least the 1,000-cell stage (3 hpf) [63, 64], this difference could explain in part, why *ezh2*-deficient zebrafish mutants develop normally. To investigate the potential contribution of *ezh2* from maternal origin in early development, we used a pharmacological approach to inhibit Ezh2 activity before zygotic genome activation. In our approach, dechorionated

embryos were exposed at the 1-2 cell stage or at 3 hpf to GSK126, a specific inhibitor of EZH2 [51]. In both cases, GSK126-mediated inhibition of maternal Ezh2 activity elicits developmental aberrations, including appearance of cardiac edemas as well as a developmental delay. Because these phenotypes were not observed in the *ezh2*-deficient zygotic mutants, we speculate that maternal Ezh2 activity contributes to zebrafish development and at least in the proper development of the heart. However, embryos exposed to GSK126 at the 1-2 cell stage gastrulate and show a normal body organization, indicating that maternal Ezh2 contributes to development but is not required for the set up of the body plan. In another study, Ostrup et al. [65] used 3-deazaneplanocin A (DZNep), an inhibitor of the S-adenosyl homocysteine hydrolase to impair Ezh2 function and H3K27me3 methylation. Zebrafish embryos treated with DZNep at the 1-2 cell stage present defects in somites, notochord and tail, resulting in abnormal body shape, as well as observed cardiac edema. Head development is also severely affected and insufficient brain segmentation, brain underdevelopment and edema are observed together with severe defects in the ear, the eye and/or in the jaw [65]. The stronger effect of DZNep, when compared to GSK126 action is probably due to the fact that DZNep may be responsible for the inhibition of other S-adenosylmethionine-dependent methyltransferases in addition to Ezh2 [66]. However, as DZNep treated and non-treated embryos develop with comparable survival rates, even upon gastrulation, this study reinforces the idea that maternal Ezh2 is not required for early development and global implementation of the body plan. Both, the role of *ezh2* in zebrafish tissue maintenance and the absence of *ezh2* requirement in the establishment of the body plan have also been demonstrated in the recent work from San et al. [60]. This study describes the generation of maternal zygotic (MZ) *ezh2* mutant embryos through germ cell transplantation. *MZezh2* mutant embryos gastrulate and form a normal body organization, but die at around 2 dpf with defects including the loss of myocardial integrity and the alteration of liver and pancreas terminal differentiation. Altogether, these data indicate that maternal *ezh2* function contributes to zebrafish development, but the loss of its activity does not block gastrulation and body plan formation.

After fertilization, the zebrafish embryonic genome is inactive till transcription is initiated during the maternal-zygotic transition, which starts around the mid-blastula transition (3.3 hpf) [64]. This transition is accompanied by the formation of pluripotent cells, the degradation of maternal transcripts and changes in epigenetic marks. In particular, H3K27me3 methylation

levels, which were low before the maternal-zygotic transition, gradually increase and numerous genes appear to be marked with H3K27me3 after this time point [67-70]. This indicates that the deposition of H3K27me3 epigenetic marks may be important after the zygotic genome activation for embryonic development. In this regard, we observed a reduction, but not the abolition of H3K27me3 methylation both in *ezh2*$^{-/-}$ mutants and in GSK126 treated embryos. This raises the possibility that Ezh1 may be able to compensate for loss of Ezh2 function, since Ezh1 also trimethylates H3K27 [71, 72]. The remaining H3K27me3 marks in *ezh2*$^{-/-}$ larvae may allow the recruitment and the action of the PRC1 complex and may explain why PRC1-deficient fish present a phenotype with more severe alterations. Indeed, *rnf2* mutant zebrafish embryos lacking PRC1 function, die at around 4-5 dpf with a normal body plan, but displaying craniofacial alterations and defects in pectoral fin development [73, 74].

During the course of our experiments, we observed the ectopic expression of *phox2bb* in the eyes of *ezh2*$^{-/-}$ mutants. Phox2bb is a homeobox-containing transcription factor often used to monitor the localization of enteric progenitors. At 5 dpf, *phox2bb* is mainly expressed in the enteric nervous system and in the hindbrain of wild-type larvae. However, additional *phox2bb* positive cells are also observed in the eyes of *ezh2*$^{-/-}$ siblings. The fact that *phox2bb* is ectopically expressed in *ezh2*-deficient larvae suggests that this gene is repressed directly or indirectly, by Ezh2. This control of *phox2bb* expression by Ezh2 appears to be also cell-specific because *phox2bb* is not ectopically expressed in all the cells and regions lacking *ezh2* expression in the mutant fish. The role of *ezh2* in *phox2bb* regulation in the eye remains unclear since *ezh2*$^{-/-}$ mutants losing the expression of *ezh2* and ectopically expressing *phox2bb* do not present histological defects in the eye. However, it is interesting to notice that this *phox2bb* ectopic expression affects limited areas in the eye, indicating that Ezh2 is not the only element controlling the expression of *phox2bb*. Furthermore, the restricted ectopic expression explains why *phox2bb* was not identified as an Ezh2 target in large scale gene expression analyses using microarrays on *MZezh2* mutants [60].

The capacities of zebrafish to regenerate some of its organs and in particular its caudal fin rely on the zebrafish ability to maintain access to a number of developmental programs and may correlate with a certain plasticity of the epigenome. In this context, it has been shown that DNA demethylation correlates with the early phase of zebrafish fin regeneration [75]. Several epigenetic factors, including components of nucleosome remodeling and deacetylase (NuRD)

complex such as *hdac1*, *mta2*, *rbb4* and *chd4a*, are also upregulated in the proliferative compartment of the blastema and required for the redifferentiation of skeletal precursors and for actinotricha formation [76]. Similarly, Stewart et al. [54] demonstrated that H3K27me3 demethylation at specific loci might be crucial to reactivate the regeneration gene expression programs and to initiate the regeneration process in response to caudal fin amputation. Here, we show that *ezh2* is expressed in regenerating caudal fin tissues after amputation both in adult and larval zebrafish. Furthermore, *ezh2*-deficient as well as wild-type larvae treated with the Ezh2 specific inhibitor GSK126, fail to properly regenerate their caudal spinal cord after transection. These results suggest that Ezh2 and H3K27me3 methylation might also be involved in processes of regeneration in zebrafish.

5. CONCLUSIONS.

In this work, we generated a zebrafish *ezh2* mutant allele using the TALEN technology. Heterozygous mutant fish are viable, fertile and do not show any obvious phenotype. In contrast to what was found in mice, homozygous *ezh2*$^{-/-}$ mutant zebrafish gastrulate properly, present a normal body plan but die at 12 dpf with defects of the intestine wall. Analysis of the intestine revealed that at 5 dpf its development is normal, but its integrity is not maintained at later developmental stages, due to enhanced cell death in *ezh2* loss-of-function mutants. Similarly, terminal differentiation of the exocrine pancreas is determined_but not fully maintained in absence of zygotic *ezh2* expression. Studies of *ezh2* expression showed that maternal *ezh2* transcripts are loaded in the embryo. At 24 hpf *ezh2* is ubiquitously expressed, whereas its expression becomes restricted to defined regions at later stages. Treatment of zebrafish embryos with the EZH2-specific inhibitor GSK126 revealed that maternal ezh2 products contribute to early development but are not required for normal body plan formation. Our results parallel and supplement those of San et al. [60] using maternal-zygotic *MZeh2* mutants. But in addition, we show that *ezh2* might play a role in the regeneration processes. Indeed, a GSK126 treatment, as well as the *ezh2* loss-of-function mutation, alters the regeneration of the chord after transection. Altogether, our work sheds light on the complex role of Ezh2 in cell fate decisions and demonstrates that zebrafish provides a remarkable model system to study Ezh2 function and H3K27me3 methylation in tissue maintenance.

ACKNOWLEDGEMENTS. We are grateful to Dr Julien Bricambert and Pr Amar Abderrahmani (CNRS UMR 8099, EGID) for providing the *ins* and *gcga* plasmids and for helpful discussions. We thank Pauline Follet for technical assistance and excellent animal care.

FUNDING. This work was supported by the Inserm, the University of Lille, the SIRIC ONCOLille, and grants from le Comité du Nord de la Ligue Contre le Cancer and l'ITMO Biologie Cellulaire, Développement et Evolution (BCDE). BD is supported by a fellowship from the Région Hauts de France Nord-Pas de Calais-Picardie and the University of Lille.

AVAILABILITY OF DATA AND METERIAL. All data generated and analyzed in this study are included in this published article and its supplementary information files.

COMPETING INTERESTS. The authors declare no competing interests.

SUPPLEMENTARY MATERIAL. Supplementary data include six figures.

REFERENCES

1. Di Croce L, Helin K. Transcriptional regulation by Polycomb group proteins. Nat. Struct. Mol Biol. 2013; 20: 1147–1155.
2. Schuettengruber B, Cavalli G. (2009). Recruitment of polycomb group complexes and their role in the dynamic regulation of cell fate choice. Development. 2009; 136: 3531–3542.
3. Surface LE, Thornton SR, Boyer LA. Polycomb group proteins set the stage for early lineage commitment. Cell Stem Cell. 2010; 7: 288–298.
4. Cao R, Wang L, Wang H, Xia L, Erdjument-Bromage H, Tempst P, Jones RS, Zhang Y. Role of histone H3 lysine 27 methylation in Polycomb-group silencing. Science. 2002; 298: 1039–1043.
5. Czermin B, Melfi R, McCabe D, Seitz V, Imhof A, Pirrotta V. Drosophila enhancer of Zeste/ESC complexes have a histone H3 methyltransferase activity that marks chromosomal Polycomb sites. Cell. 2002; 111: 185–196.
6. Kuzmichev A, Nishioka K, Erdjument-Bromage H, Tempst P, Reinberg D. Histone methyltransferase activity associated with a human multiprotein complex containing the Enhancer of Zeste protein. Genes Dev. 2002; 16: 2893–2905.
7. Margueron R, Reinberg D. The Polycomb complex PRC2 and its mark in life. Nature. 2011; 469: 343–349.
8. Müller J, Hart CM, Francis NJ, Vargas ML, Sengupta A, Wild B, Miller EL, O'Connor MB, Kingston RE, Simon JA. Histone methyltransferase activity of a Drosophila Polycomb group repressor complex. Cell. 2002; 111: 197–208.
9. Boyer LA, Plath K, Zeitlinger J, Brambrink T, Medeiros LA, Lee TI, Levine SS, Wernig M, Tajonar A, Ray MK, Bell GW, Otte AP, Vidal M, Gifford DK, Young RA, Jaenisch R. Polycomb complexes repress developmental regulators in murine embryonic stem cells. Nature. 2006; 441: 349-353.
10. Francis NJ, Kingston RE, Woodcock CL. Chromatin compaction by a polycomb group protein complex. Science. 2004; 306: 1574-1577.
11. Müller J, Verrijzer P. (2009). Biochemical mechanisms of gene regulation by polycomb group protein complexes. Curr Opin Genet Dev. 2009; 19: 150–158.
12. Wang H, Wang L, Erdjument-Bromage H, Vidal M, Tempst P, Jones RS, Zhang Y. Role of histone H2A ubiquitination in Polycomb silencing. Nature. 2004; 431: 873–878.

13. Cao R, Zhang Y. SUZ12 is required for both the histone methyltransferase activity and the silencing function of the EED-EZH2 complex. Mol Cell. 2004; 15: 57–67.
14. Pasini D, Bracken AP, Jensen MR, Lazzerini Denchi E, Helin K. Suz12 is essential for mouse development and for EZH2 histone methyltransferase activity. EMBO J. 2004; 23: 4061–4071.
15. Tie F, Stratton CA, Kurzhals RL, Harte PJ. The N terminus of Drosophila ESC binds directly to histone H3 and is required for E(Z)-dependent trimethylation of H3 lysine 27. Mol Cell Biol. 2007; 27: 2014–2026.
16. Azuara V, Perry P, Sauer S, Spivakov M, Jorgensen HF, John RM, Gouti M, Casanova M, Warnes G, Merkenschlager M, Fisher AG. Chromatin signatures of pluripotent cell lines. Nat Cell Biol. 2006; 8: 532–538.
17. Bernstein BE, Mikkelsen TS, Xie X, Kamal M, Huebert DJ, Cuff J, Fry B, Meissner A, Wernig M, Plath K, Jaenisch R, Wagschal A, Feil R, Schreiber SL, Lander ES. A bivalent chromatin structure marks key developmental genes in embryonic stem cells. Cell. 2006; 125: 315–326.
18. Bracken AP, Dietrich N, Pasini D, Hansen KH, Helin K. Genome-wide mapping of Polycomb target genes unravels their roles in cell fate transitions. Genes Dev. 2006; 20: 1123–1136.
19. Lee TI, Jenner RG, Boyer LA, Guenther MG, Levine SS, Kumar RM, Chevalier B, Johnstone SE, Cole MF, Isono K, Koseki H, Fuchikami T, Abe K, Murray HL, Zucker JP, Yuan B, Bell GW, Herbolsheimer E, Hannett NM, Sun K, Odom DT, Otte AP, Volkert TL, Bartel DP, Melton DA, Gifford DK, Jaenisch R, Young RA. Control of developmental regulators by Polycomb in human embryonic stem cells. Cell. 2006; 125: 301–313.
20. Mikkelsen TS, Ku M, Jaffe DB, Issac B, Lieberman E, Giannoukos G, Alvarez P, Brockman W, Kim TK, Koche RP, Lee W, Mendenhall E, O'Donovan A, Presser A, Russ C, Xie X, Meissner A, Wernig M, Jaenisch R, Nusbaum C, Lander ES, Bernstein BE. Genome-wide maps of chromatin state in pluripotent and lineage-committed cells. Nature. 2007; 448: 553–560.
21. Pan G, Tian S, Nie J, Yang C, Ruotti V, Wei H, Jonsdottir GA, Stewart R, Thomson JA. Whole-genome analysis of histone H3 lysine 4 and lysine 27 methylation in human embryonic stem cells. Cell Stem Cell. 2007; 1: 299–312.
22. Zhao XD, Han X, Chew JL, Liu J, Chiu KP, Choo A, Orlov YL, Sung WK, Shahab A, Kuznetsov VA, Bourque G, Oh S, Ruan Y, Ng HH, Wei CL. Whole-genome mapping of histone H3 Lys4

and 27 trimethylations reveals distinct genomic compartments in human embryonic stem cells. Cell Stem Cell. 2007; 1: 286–298.

23. Faust C, Schumacher A, Holdener B, Magnuson T. The eed mutation disrupts anterior mesoderm production in mice. Development. 1995; 121: 273–285.
24. O'Carroll D, Erhardt S, Pagani M, Barton SC, Surani MA, Jenuwein T. The polycomb-group gene Ezh2 is required for early mouse development. Mol Cell Biol. 2001; 21: 4330–4336.
25. Völkel P, Dupret B, Le Bourhis X, Angrand PO. Diverse involvement of EZH2 in cancer epigenetics. Am J Transl Res. 2015; 7: 175-193.
26. Wassef M, Margueron R. The multiple facets of PRC2 alterations in cancers. J Mol Biol. 2016; pii: S0022-2836(16)30427-2.
27. Gibson WT, Hood RL, Zhan SH, Bulman DE, Fejes AP, Moore R, Mungall AJ, Eydoux P, Babul-Hirji R, An J, Marra MA; FORGE Canada Consortium, Chitayat D, Boycott KM, Weaver DD, Jones SJ. Mutations in EZH2 cause Weaver syndrome. Am J Hum Genet. 2012; 90: 110-118.
28. Tatton-Brown K, Hanks S, Ruark E, Zachariou A, Duarte Sdel V, Ramsay E, Snape K, Murray A, Perdeaux ER, Seal S, Loveday C, Banka S, Clericuzio C, Flinter F, Magee A, McConnell V, Patton M, Raith W, Rankin J, Splitt M, Strenger V, Taylor C, Wheeler P, Temple KI, Cole T; Childhood Overgrowth Collaboration, Douglas J, Rahman N. Germline mutations in the oncogene EZH2 cause Weaver syndrome and increased human height. Oncotarget. 2011; 2: 1127-1133.
29. Tatton-Brown K, Murray A, Hanks S, Douglas J, Armstrong R, Banka S, Bird LM, Clericuzio CL, Cormier-Daire V, Cushing T, Flinter F, Jacquemont ML, Joss S, Kinning E, Lynch SA, Magee A, McConnell V, Medeira A, Ozono K, Patton M, Rankin J, Shears D, Simon M, Splitt M, Strenger V, Stuurman K, Taylor C, Titheradge H, Van Maldergem L, Temple IK, Cole T, Seal S; Childhood Overgrowth Consortium, Rahman N. Weaver syndrome and EZH2 mutations: Clarifying the clinical phenotype. Am J Med Genet A. 2013; 161A: 2972-2980.
30. Cohen AS, Yap DB,, Lewis ME, Chijiwa C, Ramos-Arroyo MA, Tkachenko N, Milano V, Fradin M, McKinnon ML, Townsend KN, Xu J, Van Allen MI, Ross CJ, Dobyns WB, Weaver DD, Gibson WT. Weaver Syndrome-Associated EZH2 Protein Variants Show Impaired Histone Methyltransferase Function In Vitro. Hum Mutat. 2016; 37: 301-307.
31. Dahlem TJ, Hoshijima K, Jurynec MJ, Gunther D, Starker CG, Locke AS, Weis AM, Voytas DF, Grunwald DJ. Simple methods for generating and detecting locus-specific mutations induced with TALENs in the zebrafish genome. PLoS Genet. 2012; 8: e1002861.

32. Bedell VM, Wang Y, Campbell JM, Poshusta TL, Starker CG, Krug RG 2nd, Tan W, Penheiter SG, Ma AC, Leung AY, Fahrenkrug SC, Carlson DF, Voytas DF, Clark KJ, Essner JJ, Ekker SC. In vivo genome editing using a high-efficiency TALEN system. Nature. 2012; 491: 114–118.

33. Moore FE, Reyon D, Sander JD, Martinez SA, Blackburn JS, Khayter C, Ramirez CL, Joung JK, Langenau DM. Improved somatic mutagenesis in zebrafish using transcription activator-like effector nucleases (TALENs). PLoS One. 2012; 7: e37877.

34. Chang N, Sun C, Gao L, Zhu D, Xu X, Zhu X, Xiong JW, Xi JJ. Genome editing with RNA-guided Cas9 nuclease in zebrafish embryos. Cell Res. 2013; 23: 465–472.

35. Hwang WY, Fu Y, Reyon D, Maeder ML, Tsai SQ, Sander JD, Peterson RT, Yeh JR, Joung JK. Efficient genome editing in zebrafish using a CRISPR-Cas system. Nat Biotechnol. 2013; 31: 227–229.

36. Xiao A, Wang Z, Hu Y, Wu Y, Luo Z, Yang Z, Zu Y, Li W, Huang P, Tong X, Zhu Z, Lin S, Zhang B. Chromosomal deletions and inversions mediated by TALENs and CRISPR/Cas in zebrafish. Nucleic Acids Res. 2013; 41: e141.

37. Kimmel CB, Ballard WW, Kimmel SR, Ullmann B, Schilling TF. Stages of embryonic development of the zebrafish. Dev Dyn. 1995; 203: 253-310.

38. Wilkinson RN, Elworthy S, Ingham PW, van Eeden FJ. A method for high-throughput PCR-based genotyping of larval zebrafish tail biopsies. Biotechniques. 2013; 55: 314-316.

39. Doyle EL, Booher NJ, Standage DS, Voytas DF, Brendel VP, Vandyk JK, Bogdanove AJ. TAL Effector-Nucleotide Targeter (TALE-NT) 2.0: tools for TAL effector design and target prediction. Nucleic Acids Res. 2012; 40: W117-122.

40. Moscou MJ, Bogdanove AJ. A simple cipher governs DNA recognition by TAL effectors. Science. 2009; 326: 1501.

41. Boch J, Scholze H, Schornack S, Landgraf A, Hahn S, Kay S, Lahaye T, Nickstadt A, Bonas U. Breaking the code of DNA binding specificity of TAL-type III effectors. Science. 2009; 326: 1509-1512.

42. Cermak T, Doyle EL, Christian M, Wang L, Zhang Y, Schmidt C, Baller JA, Somia NV, Bogdanove AJ, Voytas DF. Efficient design and assembly of custom TALEN and other TAL effector-based constructs for DNA targeting. Nucleic Acids Res. 2011; 39: e82.

43. Meeker ND, Hutchinson SA, Ho L, Trede NS. Method for isolation of PCR-ready genomic DNA from zebrafish tissues. Biotechniques. 2007; 43: 610, 612, 614.

44. Dupret B, Völkel P, Le Bourhis X, Angrand PO. The Polycomb Group Protein Pcgf1 is dispensable in zebrafish but involved in early growth and aging. PLoS One. 2016; 11: e0158700.

45. Thisse C, Thisse B. High-resolution in situ hybridization to whole-mount zebrafish embryos. Nat Protoc. 2008; 3: 59-69.

46. Brend T, Holley SA. Zebrafish whole mount high-resolution double fluorescent in situ hybridization. J Vis Exp. 2009; (25). pii: 1229.

47. Verri T, Kottra G, Romano A, Tiso N, Peric M, Maffia M, Boll M, Argenton F, Daniel H, Storelli C. Molecular and functional characterisation of the zebrafish (Danio rerio) PEPT1-type peptide transporter. FEBS Lett. 2003; 549: 115-122.

48. Ng AN, de Jong-Curtain TA, Mawdsley DJ, White SJ, Shin J, Appel B, Dong PD, Stainier DY, Heath JK. Formation of the digestive system in zebrafish: III. Intestinal epithelium morphogenesis. Dev Biol. 2005; 286: 114-135.

49. Elworthy S, Pinto JP, Pettifer A, Cancela ML, Kelsh RN. Phox2b function in the enteric nervous system is conserved in zebrafish and is sox10-dependent. Mech Dev. 2005; 122: 659–669.

50. Jülich D, Hwee Lim C, Round J, Nicolaije C, Schroeder J, Davies A, Geisler R, Lewis J, Jiang YJ, Holley SA; Tübingen 2000 Screen Consortium. beamter/deltaC and the role of Notch ligands in the zebrafish somite segmentation, hindbrain neurogenesis and hypochord differentiation. Dev Biol. 2005; 286: 391-404.

51. McCabe MT, Ott HM, Ganji G, Korenchuk S, Thompson C, Van Aller GS, Liu Y, Graves AP, Della Pietra A 3rd, Diaz E, LaFrance LV, Mellinger M, Duquenne C, Tian X, Kruger RG, McHugh CF, Brandt M, Miller WH, Dhanak D, Verma SK, Tummino PJ, Creasy CL. EZH2 inhibition as a therapeutic strategy for lymphoma with EZH2-activating mutations. Nature. 2012; 492: 108-112.

52. Xu B, Konze KD, Jin J, Wang GG. Targeting EZH2 and PRC2 dependence as novel anticancer therapy. Exp Hematol. 2015; 43: 698-712.

53. Pfefferli C, Jaźwińska A. The art of fin regeneration in zebrafish. Regeneration (Oxf). 2015; 2: 72-83.

54. Stewart S, Tsun ZY, Izpisua Belmonte JC. A histone demethylase is necessary for regeneration in zebrafish. Proc Natl Acad Sci USA. 2009; 106: 19889-19894.

55. Kawakami A, Fukazawa T, Takeda H. Early fin primordia of zebrafish larvae regenerate by a similar growth control mechanism with adult regeneration. Dev Dyn. 2004; 231: 693-699.

56. Yoshinari N, Ishida T, Kudo A, Kawakami A. Gene expression and functional analysis of zebrafish larval fin fold regeneration. Dev Biol. 2009; 325: 71-81.

57. Wallace KN, Akhter S, Smith EM, Lorent K, Pack M. Intestinal growth and differentiation in zebrafish. Mech Dev. 2005; 122: 157-173.

58. Koppens MA, Bounova G, Gargiulo G, Tanger E, Janssen H, Cornelissen-Steijger P, Blom M, Song JY, Wessels LF, van Lohuizen M. Deletion of Polycomb Repressive Complex 2 From Mouse Intestine Causes Loss of Stem Cells. Gastroenterology. 2016; 151: 684-697.

59. Pack M, Solnica-Krezel L, Malicki J, Neuhauss SC, Schier AF, Stemple DL, Driever W, Fishman MC. Mutations affecting development of zebrafish digestive organs. Development. 1996; 123: 321-328.

60. San B, Chrispijn ND, Wittkopp N, van Heeringen SJ, Lagendijk AK, Aben M, Bakkers J, Ketting RF, Kamminga LM. Normal formation of a vertebrate body plan and loss of tissue maintenance in the absence of ezh2. Sci Rep. 2016; 6: 24658.

61. Hobert O, Sures I, Ciossek T, Fuchs M, Ullrich A. Isolation and developmental expression analysis of Enx-1, a novel mouse Polycomb group gene. Mech Dev. 1996; 55: 171-184.

62. Ningxia Z, Shuyan L, Zhongjing S, Ling C, Tianzhong M, Lifeng W, Yan Y, Leili L, Xiancai C, Haibin C. The expression pattern of polycomb group protein Ezh2 during mouse embryogenesis. Anat Rec (Hoboken). 2011; 294: 1150-1157.

63. Mathavan S, Lee SG, Mak A, Miller LD, Murthy KR, Govindarajan KR, Tong Y, Wu YL, Lam SH, Yang, Ruan Y, Korzh V, Gong Z, Liu ET, Lufkin T. Transcriptome analysis of zebrafish embryogenesis using microarrays. PLoS Genet. 2005; 1: 260-276.

64. Tadros W, Lipshitz HD. The maternal-to-zygotic transition: a play in two acts. Development. 2009; 136: 3033-3042.

65. Ostrup O, Reiner AH, Alestrom P, Collas P. The specific alteration of histone methylation profiles by DZNep during early zebrafish development. Biochim Biophys Acta. 2014; 1839: 1307-1315.

66. Miranda TB, Cortez CC, Yoo CB, Liang G, Abe M, Kelly TK, Marquez VE, Jones PA. DZNep is a global histone methylation inhibitor that reactivates developmental genes not silenced by DNA methylation. Mol Cancer Ther. 2009; 8: 1579–1588.

67. Vastenhouw NL, Zhang Y, Woods IG, Imam F, Regev A, Liu XS, Rinn J, Schier AF. Chromatin signature of embryonic pluripotency is established during genome activation. Nature. 2010; 464: 922-926.

68. Lindeman LC, Andersen IS, Reiner AH, Li N, Aanes H, Østrup O, Winata C, Mathavan S, Müller F, Aleström P, Collas P. Prepatterning of developmental gene expression by modified histones before zygotic genome activation. Dev Cell. 2011; 21: 993-1004.

69. Andersen IS, Lindeman LC, Reiner AH, Østrup O, Aanes H, Aleström P, Collas P. Epigenetic marking of the zebrafish developmental program. Curr Top Dev Biol. 2013; 104: 85-112.

70. Andersen IS, Ostrup O, Lindeman LC, Aanes H, Reiner AH, Mathavan S, Aleström P, Collas P. Epigenetic complexity during the zebrafish mid-blastula transition. Biochem Biophys Res Commun. 2012; 417: 1139-1144.

71. Shen X, Liu Y, Hsu YJ, Fujiwara Y, Kim J, Mao X, Yuan GC, Orkin SH. EZH1 mediates methylation on histone H3 lysine 27 and complements EZH2 in maintaining stem cell identity and executing pluripotency. Mol Cell. 2008; 32: 491-502.

72. Margueron R, Li G, Sarma K, Blais A, Zavadil J, Woodcock CL, Dynlacht BD, Reinberg D. Ezh1 and Ezh2 maintain repressive chromatin through different mechanisms. Mol Cell. 2008; 32: 503-518.

73. van der Velden YU, Wang L, van Lohuizen M, Haramis AP. The Polycomb group protein Ring1b is essential for pectoral fin development. Development. 2012; 139: 2210-2220.

74. van der Velden YU, Wang L, Querol Cano L, Haramis AP. The polycomb group protein ring1b/rnf2 is specifically required for craniofacial development. PLoS One. 2013; 8: e73997.

75. Hirose K, Shimoda N, Kikuchi Y. Transient reduction of 5-methylcytosine and 5-hydroxymethylcytosine is associated with active DNA demethylation during regeneration of zebrafish fin. Epigenetics. 2013; 8: 899-906.

76. Pfefferli C, Müller F, Jazwinska A, Wicky C. Specific NuRD components are required for fin regeneration in zebrafish. BMC Biology. 2014; 12: 1-17.

FIGURE LEGENDS

Figure 1. Generation of ezh2 mutant zebrafish using the TALEN technology. (**A**) Schematic representation of the genomic structure of the *ezh2* gene, with coding and untranslated exons depicted as solid and open boxes, respectively. The exonic regions coding for the conserved SANT and SET domains are shown in red and brown, respectively. The location of the *ezh2* TALEN in exon 2 is indicated. The *ezh2* TALEN target sequence with Left and Right TALEN binding sites in red is shown. The DdeI restriction site is indicated in green. (**B**) Identification of mutant embryos using a diagnostic restriction. Genomic DNA was prepared from an uninjected (Control) and an *ezh2* TALEN injected (TAL-ezh2) embryo. The TALEN targeted DNA region is amplified by PCR and subjected to DdeI digestion. The TAL-ezh2 injected embryo contains undigested material (arrow at 466 bp), indicating that the DdeI diagnostic restriction site has been disrupted. (**C**) Sequence of the mutant allele compared to its wild-type counterpart. Small letters indicate inserted nucleotides. The mutated *ezh2* allele (Mut) contains a 22 bp net insertion resulting from a deletion of 5 nucleotides (underlined in the wild-type sequence) and an insertion of 27 nucleotides (small letters). (**D**) Schematic representation of the wild-type ($Ezh2^{wt}$) and mutant ($Ezh2^{mut}$) proteins. The gray line in the predicted mutant protein indicates residues read out of frame prior to encountering a premature stop codon, whereas the red and brown motifs in the wild-type protein correspond to SANT (SMART: SM00717) and SET (SMART: SM00317) domains, respectively. Size of the predicted proteins is indicated.

Figure 2. Loss of Ezh2 function does not affect early zebrafish development. (**A**) At 5 dpf, $ezh2^{-/-}$ mutants from $ezh2^{+/-}$ crosses are phenotypically indistinguishable from heterozygous and wild-type siblings. (**B**) Alcian blue stained head cartilages of $ezh2^{+/+}$ (up) and $ezh2^{-/-}$ (down) siblings at 6 dpf reveal that craniofacial cartilage development is not affected in $ezh2^{-/-}$ mutants. cb: ceratobranchials; ch: ceratohyal; ep: ethmoid plate; m: Meckel's cartilage; n: notochord; ot: otoliths; pq: palatoquadrate. (**C**) Cranial musculature revealed by immunocytochemistry using the anti-myosin MF20 antibody shows that muscle development is normal in $ezh2^{-/-}$ fish at 6 dpf. adm: adductor mandibulae; ao: adductor operculi; bm: branchial musculatur; do: dilatator operculi; hi: hyoideus inferior; hs: hyoideus superior; ima:

intermandibularis anterior; imp: intermandibularis posterior; lo: levator operculi; pf: pectoral fin; sh: sternohyoideus.

Figure 3. ezh2 expression in ezh2$^{+/+}$and ezh2$^{-/-}$ siblings at different developmental time points. (**A**) *In situ* hybridization at the 1- and 2-cell stages showing that *ezh2* mRNA is maternally provided in zebrafish embryos. (**B**) The analysis of *ezh2* transcripts by RT-PCR at 2 hpf shows that wild-type, but not mutant transcripts are delivered into the embryos from *ezh2*$^{+/-}$ crosses (♂x♀ *ezh2*$^{+/-}$). Ezh2 transcripts from *ezh2*$^{+/+}$ crosses are shown on the left part (WT). By RT-PCR, wild-type *ezh2* mRNA is expected to give a band at 328 bp, whereas the size of the mutant transcript should be at 350 bp. After DdeI digestion, the predicted restriction fragments from the wild-type cDNA will be at 171, 122, 31 and 4 bp, while those from the mutant will be at 315, 31 and 4 bp. Relative mRNA abundance is shown by RT-PCR amplification of the *β-actin* mRNAs (act) (**C**) *In situ* hybridization to detect *ezh2* transcripts in *ezh2*$^{+/+}$ (left) and *ezh2*$^{-/-}$ (right) siblings from *ezh2*$^{+/-}$ crosses at the indicated time points. (**D**) Lateral view of 96 hpf *ezh2*$^{+/+}$ (left) and *ezh2*$^{-/-}$ (right) siblings showing *ezh2* expression detected by *in situ* hybridization in the intestine of wild-type larvae (arrow). Scale bar is 500 µm.

Figure 4. Ezh2 is required for maintenance of the intestine integrity in zebrafish. (**A**) Representative images of lateral views of *ezh2*$^{+/+}$ and *ezh2*$^{-/-}$ larvae as indicated, stained with oil Red-O at 9 dpf. On the enlarged picture, the liver is indicated by an asterisk. The intestine wall appears well defined and finer in *ezh2*$^{-/-}$ mutants (arrow). Scale bar is 500 µm, or 200 µm on the enlargement panels. (**B**) Intestinal sections from *ezh2*$^{+/+}$ and *ezh2*$^{-/-}$ larvae immunostained for actin and counterstained with hematoxylin, at 5 dpf (left) and 9 dpf (right). Scale bar is 100 µm. (**C**) TUNEL assay on sections from the intestinal bulb of *ezh2*$^{+/+}$ (left) and *ezh2*$^{-/-}$ (right) larvae at 9 dpf, showing an increase of apoptosis levels in the intestine and the pancreas (asterisk) in *ezh2*$^{-/-}$ mutants. Scale bar is 100 µm.

Figure 5. Ectopic expression of phox2bb in the eyes of ezh2 mutants. (**A**) *In situ* hybridization showing that the localization of *phox2bb* expressing neural crest cells along the gut (arrow) is not altered by loss of Ezh2 function at 5 dpf. (**B**) Expression of *ezh2* (up) and *phox2bb* (down) in the anterior region of *ezh2*$^{+/+}$ (left) and *ezh2*$^{-/-}$ (right) siblings at 5dpf, as shown by *in situ*

hybridization. Expression of *ezh2* in *ezh2*$^{+/+}$ and *phox2bb* in *ezh2*$^{-/-}$ larvae respectively, is outlined by arrows. (**C**) Lateral view of *ezh2* expression in *ezh2*$^{+/+}$ larvae (up) and *phox2bb* expression in *ezh2*$^{-/-}$ larvae (down) at 5 dpf in the eye. (**D**) Detection of the *ezh2* mRNA by *in situ* hybridization using a digoxygenin-labeled riboprobe and tyramide signal amplification-Cy5 reagent before eye section on wild-type larvae at 9 dpf. abc: amacrine and bipolar cells; c: cornea; gc: ganglion cells; ip: Inner plexiform; l: lens; op: outer plexiform; pr: photoreceptors; rpe: retinal pigmented epithelium. Scale bar is 100 µm. (**E**) Hematoxylin-eosin staining of eye sections of *ezh2*$^{+/+}$ (left) and *ezh2*$^{-/-}$ (right) siblings at 9 dpf. abc: amacrine and bipolar cells; c: cornea; gc: ganglion cells; ip: Inner plexiform; l: lens; op: outer plexiform; rpe: retinal pigmented epithelium. Scale bar is 100 µm.

Figure 6. The exocrine pancreas development is affected in ezh2*$^{-/-}$ *mutants. (**A**) *In situ* hybridization for different markers of the pancreas in *ezh2*$^{+/+}$ (left) and *ezh2*$^{-/-}$ (right) siblings from *ezh2*$^{+/-}$ crosses, performed at 5 dpf. No difference is found for markers of the endocrine pancreas (*ins* and *gcga*, arrow), whereas *try*, a marker for terminal differentiation of the exocrine pancreas reveals a reduced signal area in *ezh2*$^{-/-}$ larvae. Representative fish of each genotype are shown. Scale bar is 500 µm. (**B**) *In situ* hybridization at 3 dpf showing that the *try* signal is similar in *ezh2*$^{+/+}$ (left) and *ezh2*$^{-/-}$ (right) siblings. Scale bar is 500 µm.

Figure 7. Global trimethylation of lysine 27 of histone H3 is reduced in ezh2*$^{-/-}$ *mutants. After genotyping of the caudal region of the larvae, total histones from pools of 5 larvae of *ezh2*$^{+/+}$ and *ezh2*$^{-/-}$ genotypes at 9 and 12 dpf (**A**) or from *ezh2*$^{+/+}$, *ezh2*$^{+/-}$ and *ezh2*$^{-/-}$ genotypes at 9 dpf (**B**) as indicated, were extracted and analyzed by western blotting using a specific anti-H3K27me3 antibody and an anti-H3 antibody as a control. (**C**) Immunostaining for H3K27me3 in wildtype and *ezh2*$^{-/-}$ embryos as indicated at 24 hpf (left) and 4 dpf (right). Scale bars are 500 µm and 1 mm for 24 hpf embryos and 4 dpf larvae, respectively.

Figure 8. GSK126 elicits developmental aberrations in zebrafish. (**A**) Scoring of abnormal and dead embryos at 24 and 96 hpf. Embryos were exposed to 1 µM GSK126 (n=397) or to 0.01% DMSO (n=114) at 3 hpf. (**B**) Representative phenotype of embryos and larvae without treatment (DMSO 0.01%) or treated with 1 µM GSK126 at the indicated time points. Notice cardiac edemas (arrows) and absence of pectoral fins at 96 hpf. Scale bar is 500 µm. (**C**)

Measurement of the size of the eye in 96 hpf larvae without treatment (DMSO 0.01%) or treated with 1 µM GSK126. Statistical significance was assessed by a Student t-test analysis and the significance is expressed as the indicated p value. (**D**) Global trimethylation of lysine 27 of histone H3 assayed by western blotting using a specific anti-H3K27me3 antibody and an anti-H3 antibody as control. Quantified relative H3K27me3 levels normalized to levels of histone H3 are indicated. (**E**) Whole mount immunostaining for H3K27me3 in wildtype embryos treated with 1 µM GSK126 or control (DMSO 0.01%) as indicated, at 4 dpf. Scale bar is 1 mm.

Figure 9. Ezh2 and larval caudal fin regeneration. (**A**) *In situ* hybridization to visualize *ezh2* expression on a representative control untransected zebrafish larvae at 5 dpf (top) and on a representative larval fin at 5 dpf, 2 days post-amputation (bottom). Ezh2 expression is detected in regenerating tissues (arrow head). (**B**) The Ezh2 specific inhibitor GSK126 affects larval caudal fin regeneration. At 3 dpf (a, a'), the tip of the caudal fin of wild-type larvae is sectioned within the pigment gap distal to the circulating blood (b, b') and embryos were subsequently treated with 1 µM GSK126 or with 0.01 % DMSO (control). At 2 days post-amputation the spinal cord regeneration is inhibited in the treated larvae (c'), but not in the controls (c). The dotted line indicates the transection site. (**C**) Ezh2 function is required for spinal cord regeneration. At 3 dpf (a, a'), the tip of the caudal fin of wild-type (*ezh2*$^{+/+}$) or Ezh2-deficient (*ezh2*$^{-/-}$) siblings is sectioned within the pigment gap distal to the circulating blood (b, b'). Two days after the transection, spinal cord regeneration is reduced in mutant larvae (c') compared to wild-type (c). The dotted line indicates the transection site.

A

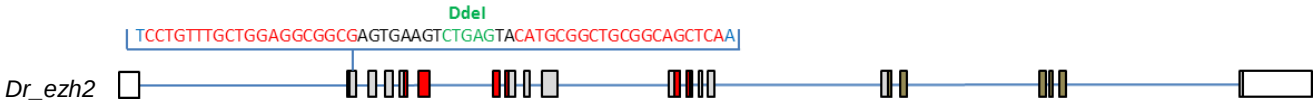

B

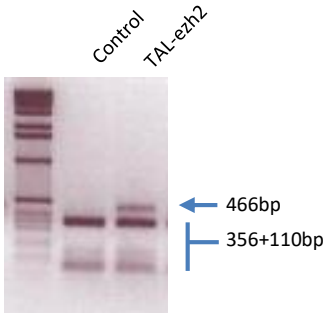

C

DdeI

```
WT  TCCTGTTTGCTGGAGGCGGCGAGTGAAGTCTGAGTACATGCGGCTGCGGCAGCTCAACGCTTCAGGAGGGCAG
Mut TCCTGTTTGCTGGAGGCGGCGAGTGAcatgcgaaaaacatgcgaaagacatgcGAGTACATGCGGCTGCGGCAGCTCAA  +22 (Δ5, +27)
```

D

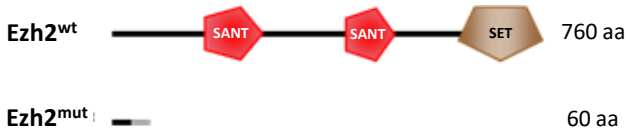

Dupret et al. – Figure 1

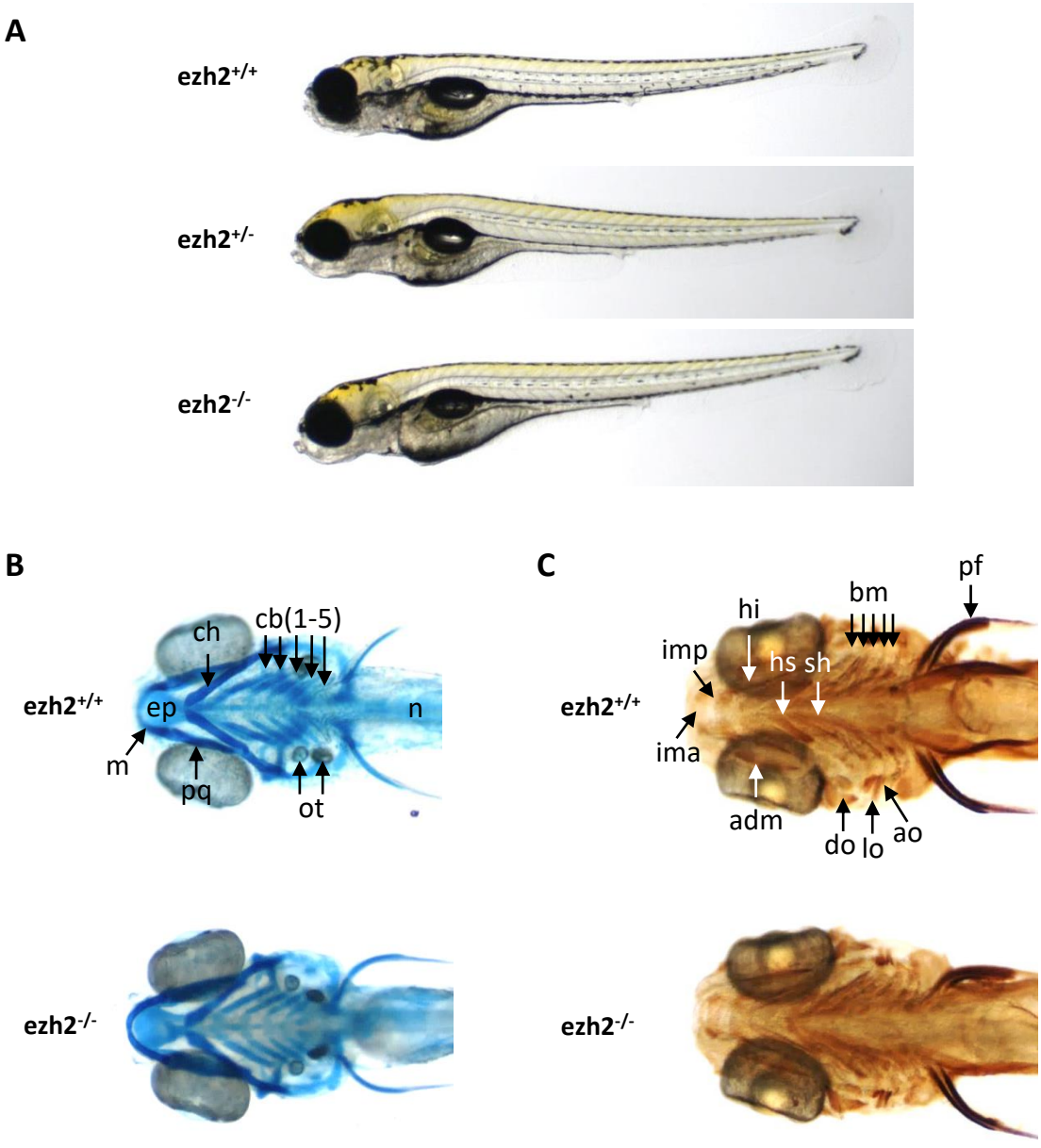

Dupret et al. – Figure 2

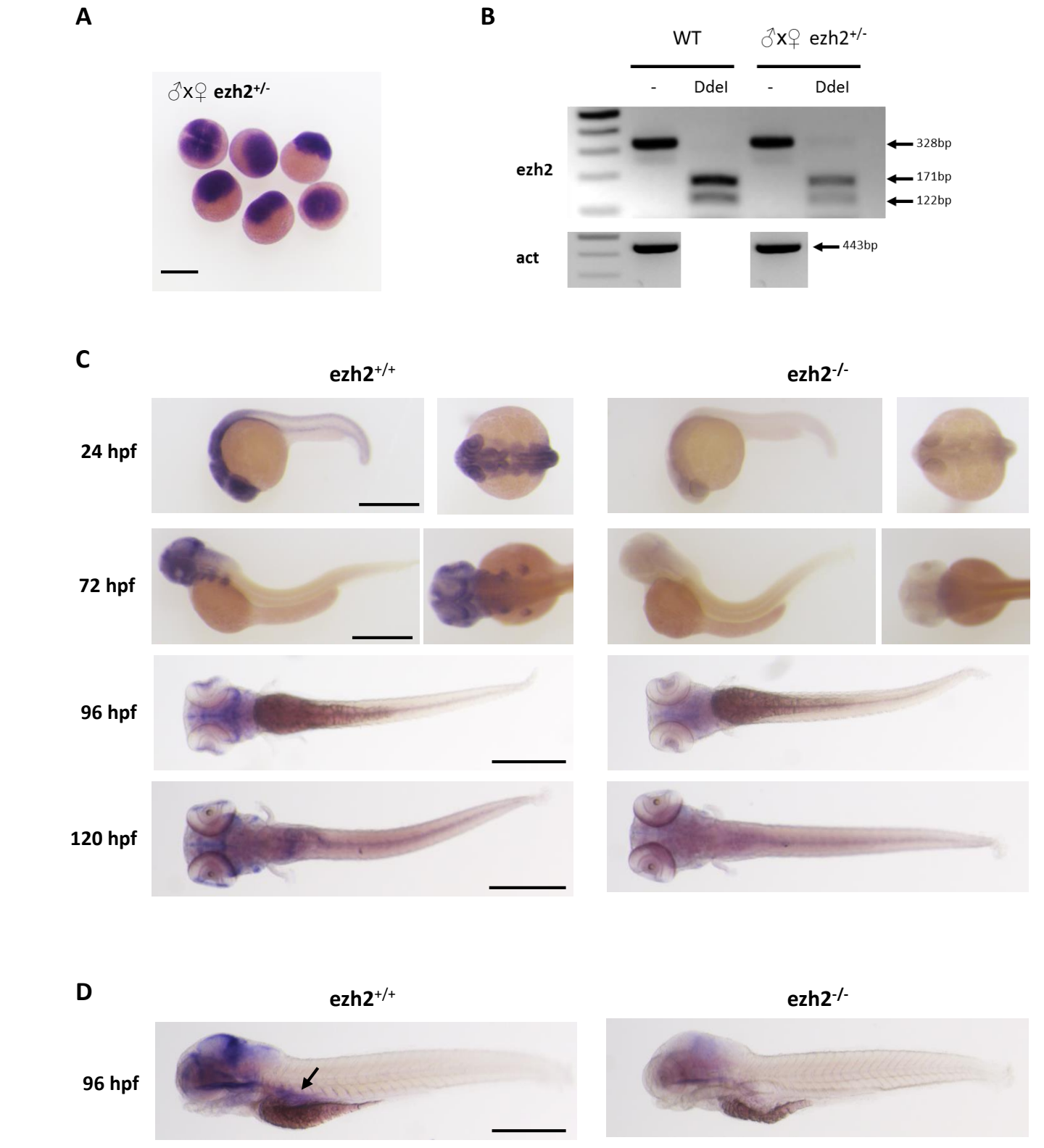

Dupret et al. – Figure 3

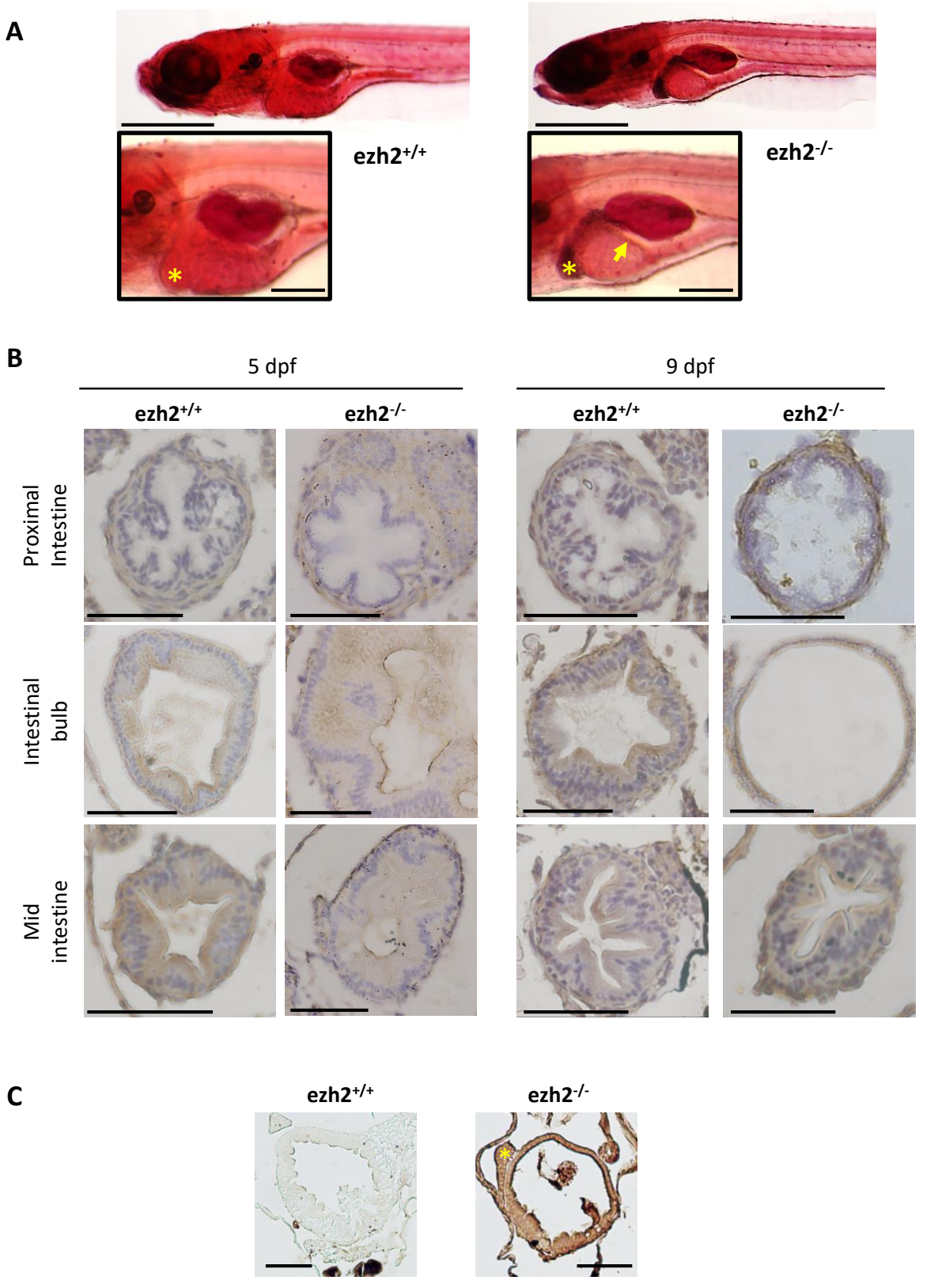

Dupret et al. – Figure 4

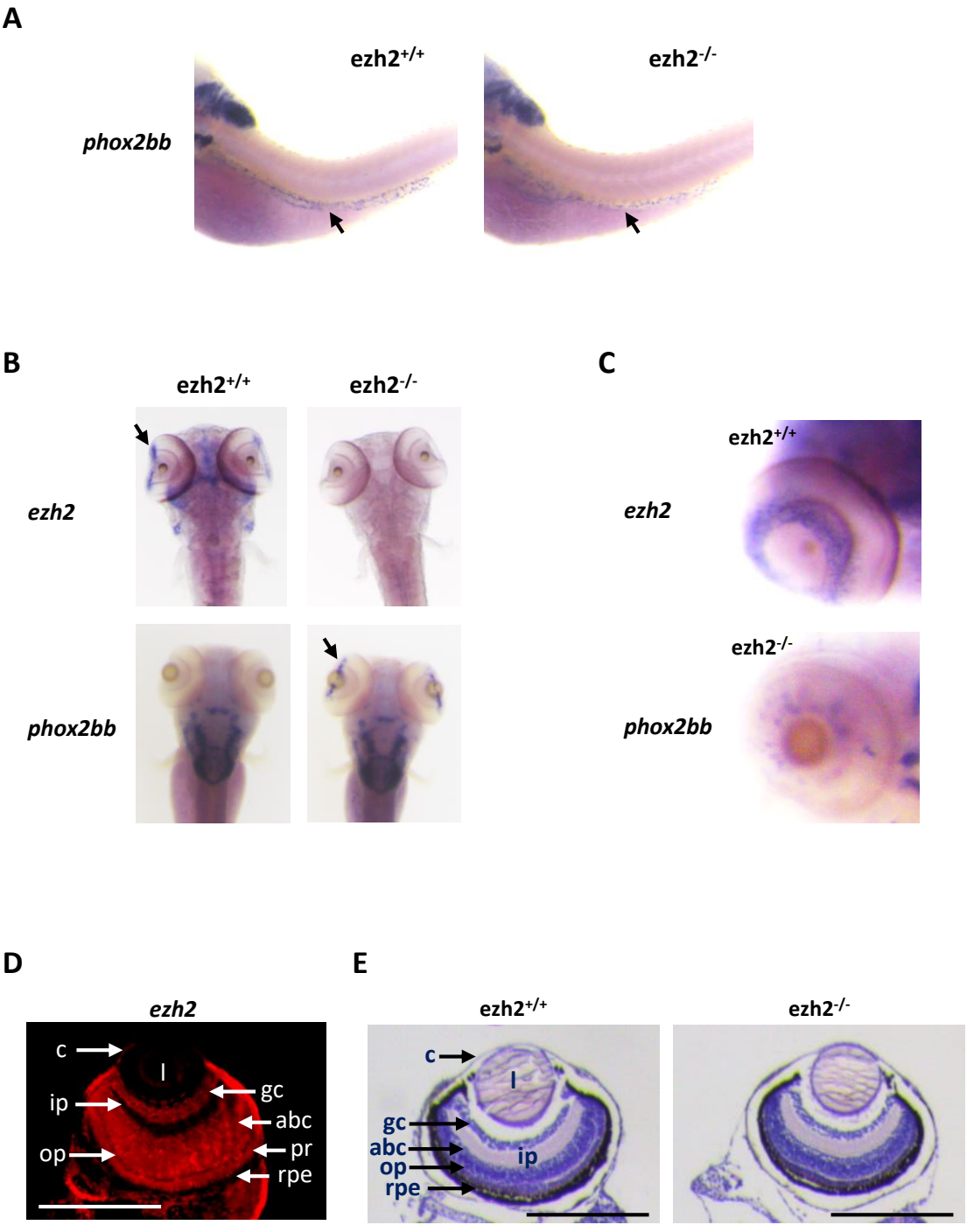

Dupret et al. – Figure 5

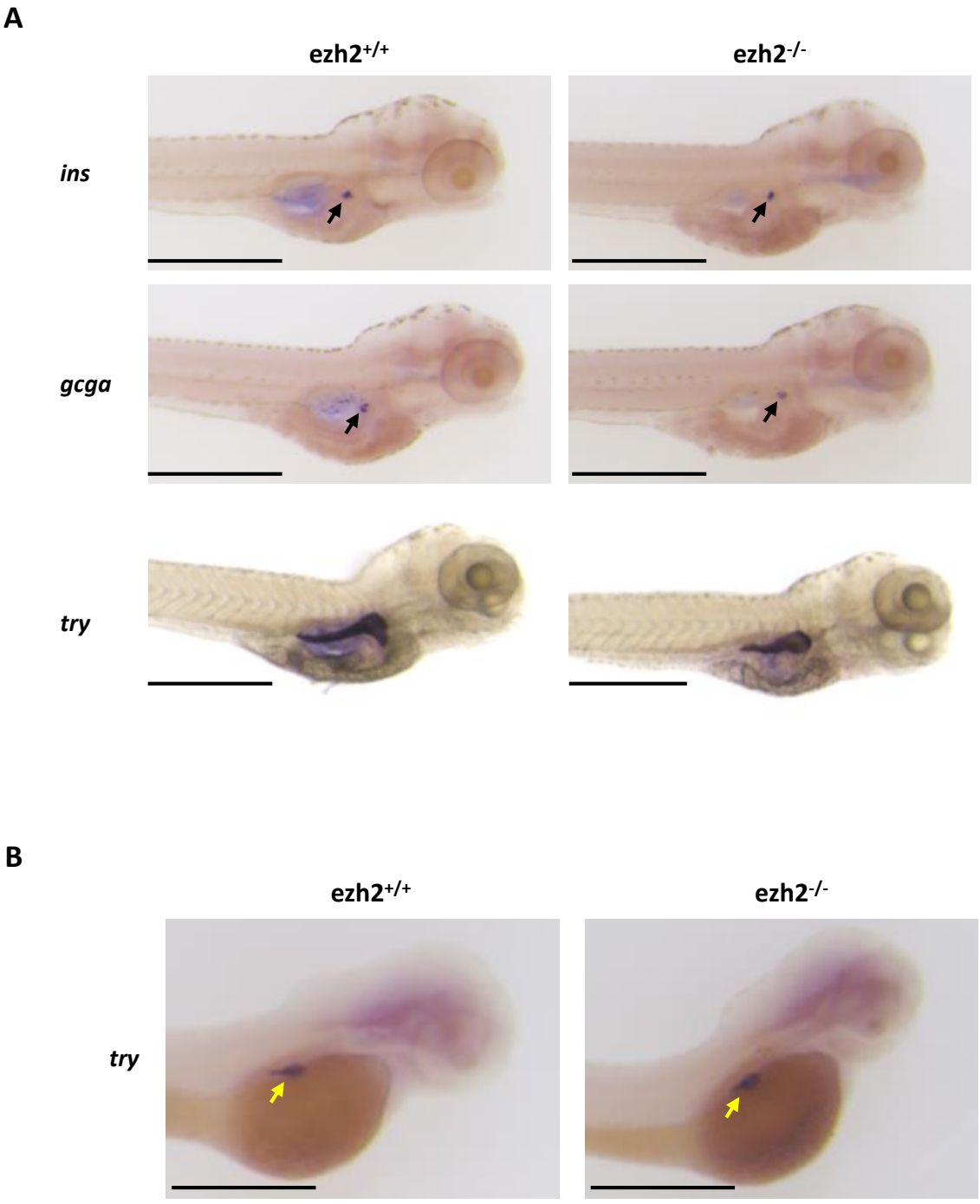

Dupret et al. – Figure 6

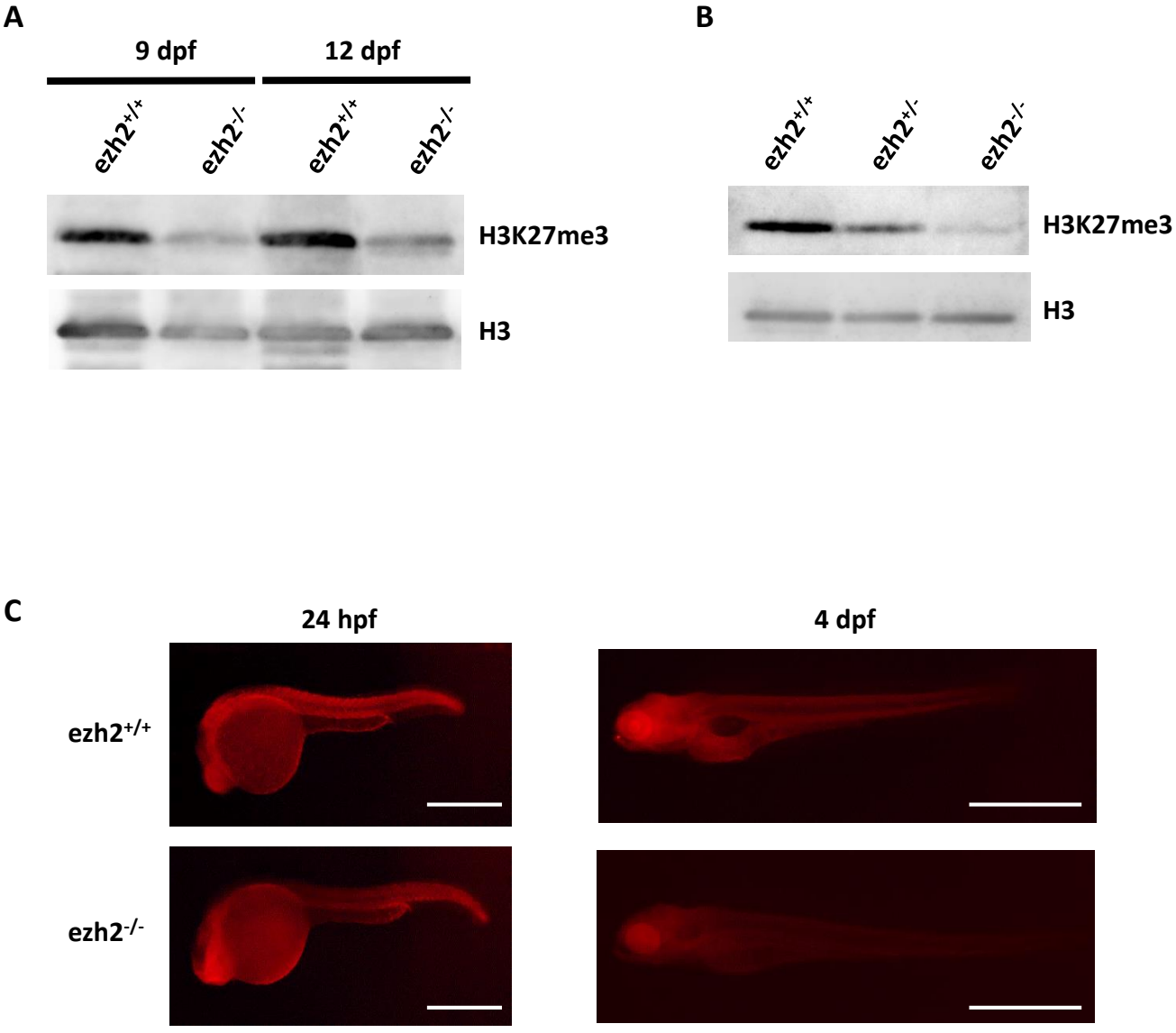

Dupret et al. – Figure 7

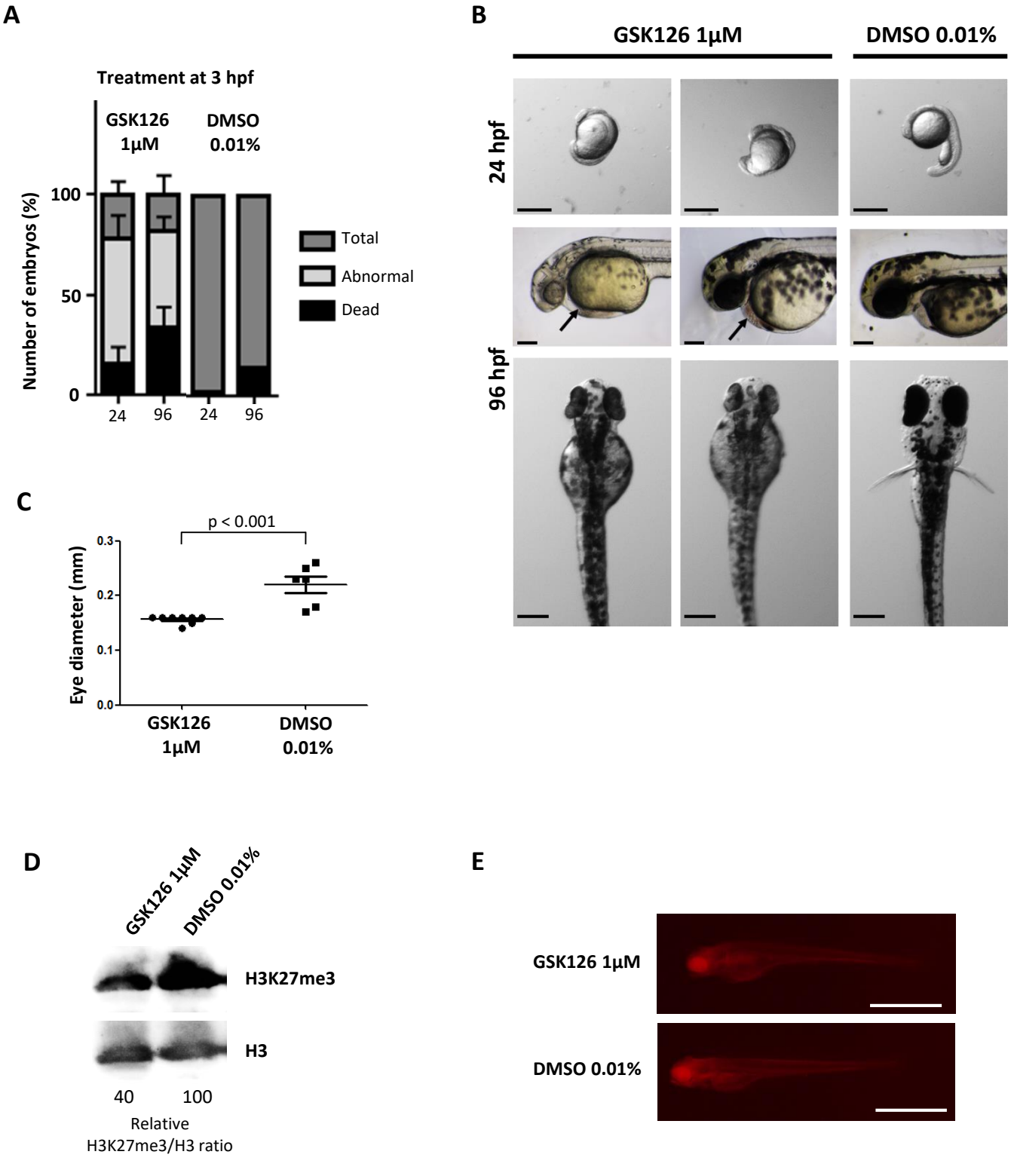

Dupret et al. – Figure 8

A

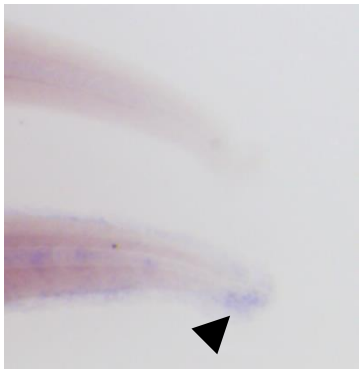

B

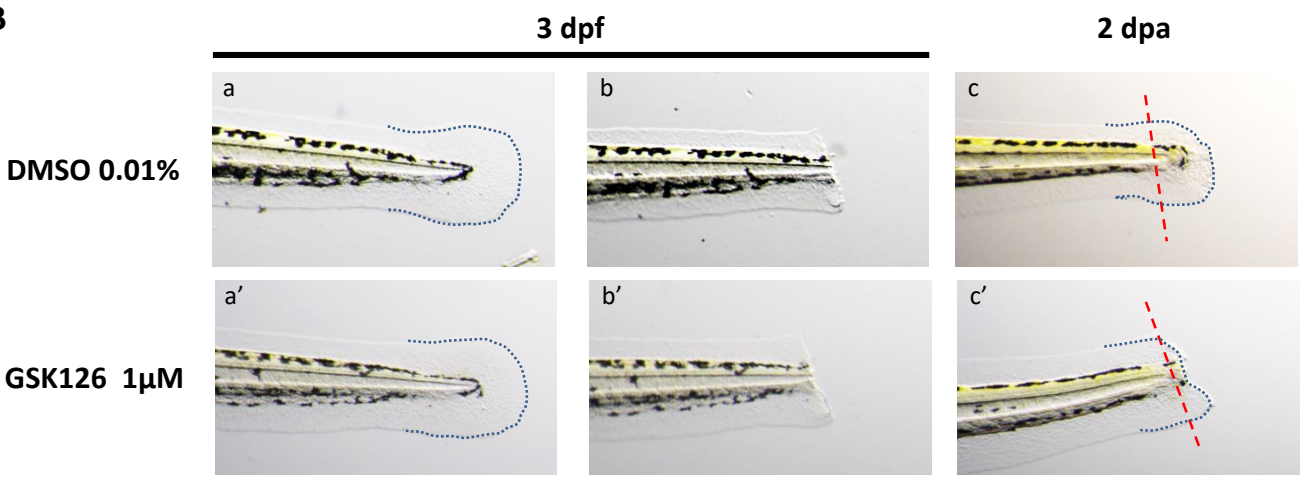

C

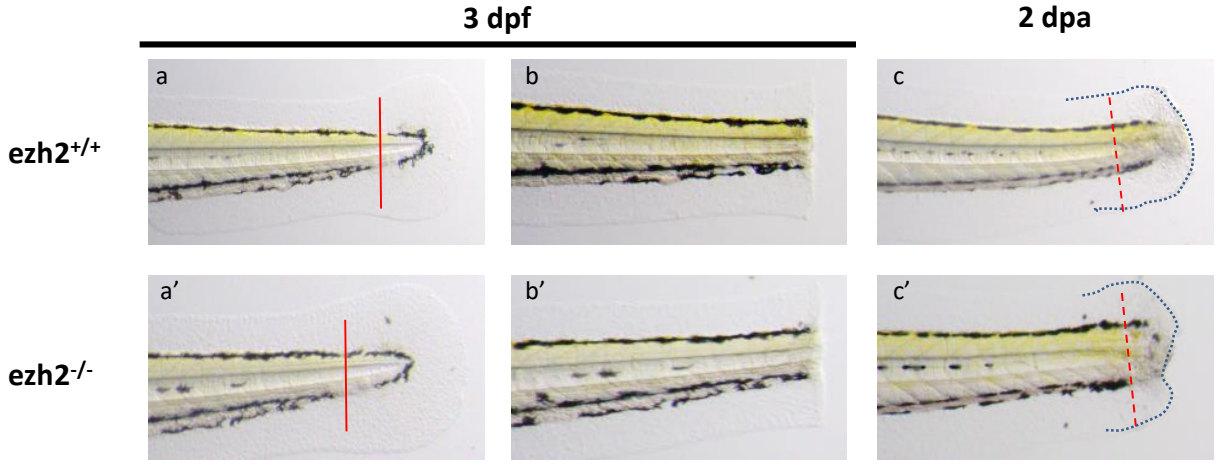

Dupret et al. – Figure 9

The histone lysine methyltransferase Ezh2 is required for maintenance of the intestine integrity and for caudal fin regeneration in zebrafish

Barbara Dupret, Pamela Völkel, Constance Vennin, Robert-Alain Toillon, Xuefen Le Bourhis and Pierre-Olivier Angrand*

SUPPLEMENTARY DATA

Supplementary Figure S1. Product of the ezh2 mutant allele. Predicted protein encoded by the ezh2 mutant allele ($Ezh2^{mut}$) compared to the wild-type Ezh2 ($Ezh2^{wt}$) protein. Peptides coding for the conserved SANT and SET domains are indicated in red and brown, respectively.

Supplementary Figure S2. ezh2 mRNAs in ezh2$^{+/+}$and ezh2$^{-/-}$ zebrafish. (**A**) Detection of *ezh2* transcripts in the intestine by *in situ* hybridization using a digoxygenin-labeled riboprobe and tyramide signal amplification-Cy5 reagent (red) before section of wild-type larvae at 5 dpf. DNA was counterstained by Hoechst 33342 (blue). L: lumen. Scale bar is 100 µm. (**B**) Relative abundance of *ezh2* transcripts in wild-type embryos at the indicated time points, measured by RT-PCR using primers located in exons 1 and 3 showing that *ezh2* mRNA abundance decreases during development. Total mRNA abundance is shown by RT-PCR amplification of the β-actin mRNAs (act). (**C**) RT-PCR analysis reveals that the *ezh2* mRNAs present in *ezh2*$^{-/-}$ embryos from *ezh2*$^{+/-}$ crosses correspond to zygotic transcripts, rather than to maternally deposited mRNAs. By RT-PCR using the primers designed in exons 1 and 3, wild-type *ezh2* transcripts are expected to give a band at 328 bp, whereas the size of the mutant transcript should be at 350 bp. After DdeI digestion, the predicted restriction fragments derived from the mutant cDNAs will be at 315, 31 and 4 bp. The mRNAs used in the RT-PCR experiment were extracted from 3 dpf old *ezh2*$^{+/+}$ (WT) and *ezh2*$^{-/-}$ siblings coming from *ezh2*$^{+/-}$ in-crosses. (**D**) Chromatogram showing the sequence of the *ezh2* cDNA generated by RT-PCR from mRNAs extracted from 3 dpf old *ezh2*$^{-/-}$ embryos. The sequence corresponds to the mutant transcript,

but not to the wild-type one. Parts of Left and Right TALEN binding sites are shown in red and the 27 nt insertion in small letters.

Supplementary Figure S3. Structure of the ezh2$^{-/-}$ intestine. (**A**) Hematoxylin-eosin staining of serial sections of *ezh2*$^{-/-}$ larvae at 11 dpf showing the alteration of the intestine wall in the bulb region but not in the more proximal and distal parts. Scale bar is 200 µm. (**B**) Transverse sections through the intestinal bulb of *ezh2*$^{+/+}$ and *ezh2*$^{-/-}$ siblings at 5 and 10 dpf, as indicated, incubated with rhodamine phalloidin to stain F-actin (red) and Hoechst 33342 to stain DNA (blue). Scale bar is 100 µm.

Supplementary Figure S4. Reduced exocrine pancreas in ezh2$^{-/-}$ mutants. (**A**) *In situ* hybridization for the exocrine pancreas terminal differentiation marker *try*, in *ezh2*$^{+/+}$ (left) and *ezh2*$^{-/-}$ (right) siblings at 5 dpf. (**B**) Quantification of the *try* signal using Adobe Photoshop in *ezh2*$^{+/+}$ and *ezh2*$^{-/-}$ larvae. Statistical significance was assessed by a Student t-test analysis and significance expressed as the indicated p value.

Supplementary Figure S5. GSK126 treatment at the 1-2 cell stage elicits developmental alterations in zebrafish. (**A**) Representative phenotype of embryos and larvae without treatment (DMSO 0.01%) or treated with 1 µM GSK126 at the indicated time points. Note the absence of pectoral fins at 72 hpf and cardiac edemas (arrows) at 96 hpf. Scale bar is 500 µm. (**B**) Global trimethylation of lysine 27 of histone H3 assayed by western blotting using a specific anti-H3K27me3 antibody and an anti-H3 antibody as a control. Quantified relative H3K27me3 levels normalized to levels of histone H3 are indicated.

Supplementary Figure S6. Expression of ezh2 in regenerating caudal fin. Whole-mount *in situ* hybridization of regenerating caudal fins at 4 days post-amputation (dpa) using an anti-sense (up) or a sense (down) *ezh2* probe performed on 6 months old wild-type (TU) fish.

Ezh2^{wt}

MGLTGRKSEKGPVCWRRRVKSEYMRLRQLKRFRRADEVKSMFSS
NRQKILERTDILNQEWKLRRIQPVHIMTPVSSLRGTRECTVDSG
FSEFSRQVIPLKTLNAVASVPVMYSWSPLQQNFMVEDETVLHNI
PYMGDEILDQDGTFIEELIKNYDGKVHGDRECGFINDEIFVELV
NALNQYSDNEEDDEEDDHHDYKFEKMDLCDGKDDAEDHKEQLSS
ESHNNDGSKKFPSDKIFEAISSMFPDKGSTEELKEKYKELTEQQ
LPGALPPECTPNIDGPNAKSVQREQSLHSFHTLFCRRCFKYDCF
LHPFQATPNTYKRKNMENLVDSKPCGIYCYMYMVQDGMVREYPA
GVVPERAKTPSKRSTGRRRGRLPNSNSRPSTPTVNSETKDTDSD
REGGADGNDSNDKDDDDKKDETTSSSEANSRCQTPVKLKLSSEP
PENVDWSGAEASLFRVLIGTYYDNFCAIARLIGTKTCRQVYEFR
VKESSIIARAPAVDENTPQRKKKRKHRLWATHCRKIQLKKDGSS
NHVYNYQPCDHPRQPCDSSCPCVTAQNFCEKFCQCSSECQNRFP
GCRCKAQCNTKQCPCYLAVRECDPDLCLTCGAAEHWDSKNVSCK
NCSIQRGAKKHLLLAPSDVAGWGIFIKEPVQKNEFISEYCGEII
SQDEADRRGKVYDKYMCSFLFNLNNDFVVDATRKGNKIRFANHS
VNPNCYAKVMMVNGDHRIGIFAKRAIQTGEELFFDYRYSQADAL
KYVGIEREMEIP*

Ezh2^{mut}

MGLTGRKSEKGPVCWRRRV↓TCEKHAKDMRVHAAAAAQTLQEGR
RGQEHVQLQQTKNTGAY*

Dupret et al. – Additional Figure S1

A

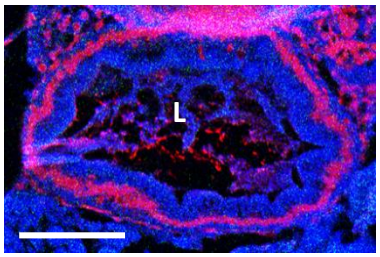

B

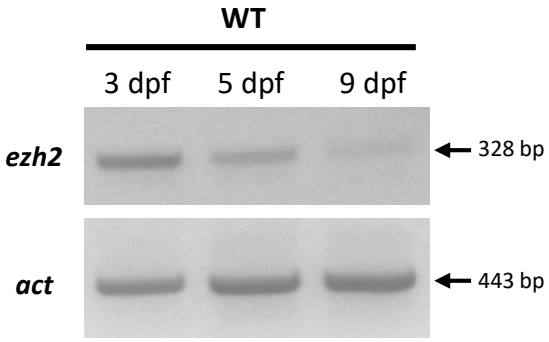

C

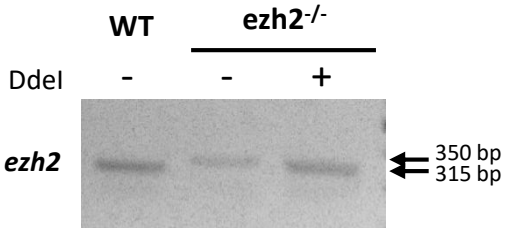

D

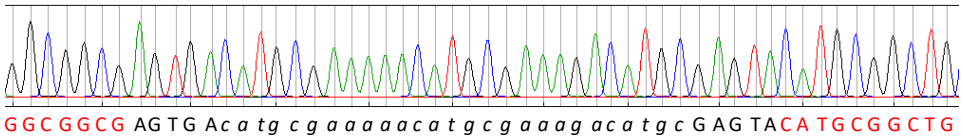

Dupret et al. – Additional Figure S2

A

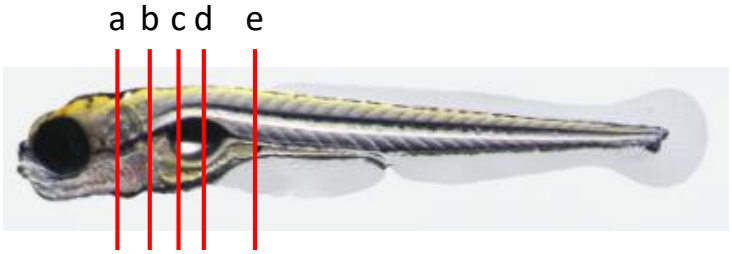

Ezh2$^{-/-}$ 11 dpf

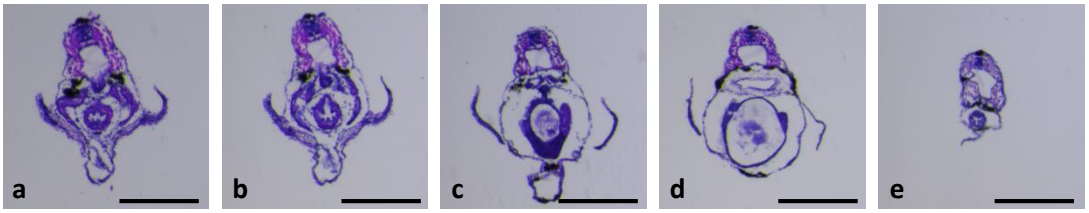

B

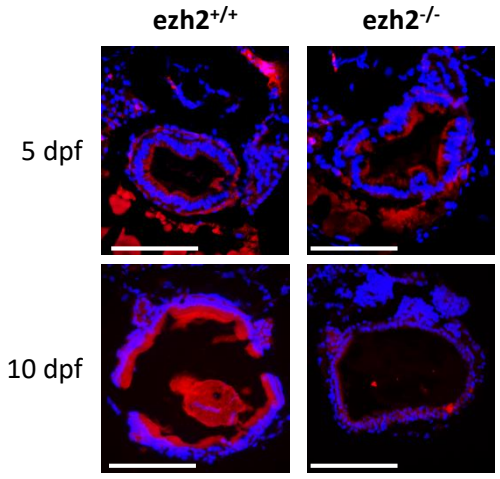

Dupret et al. – Additional Figure S3

A

B

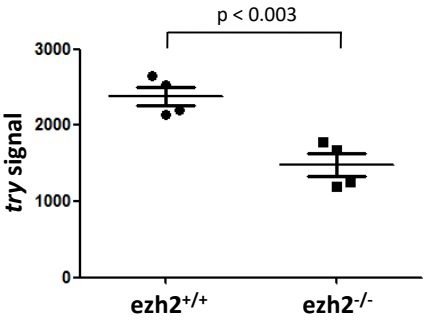

Dupret et al. – Additional Figure S4

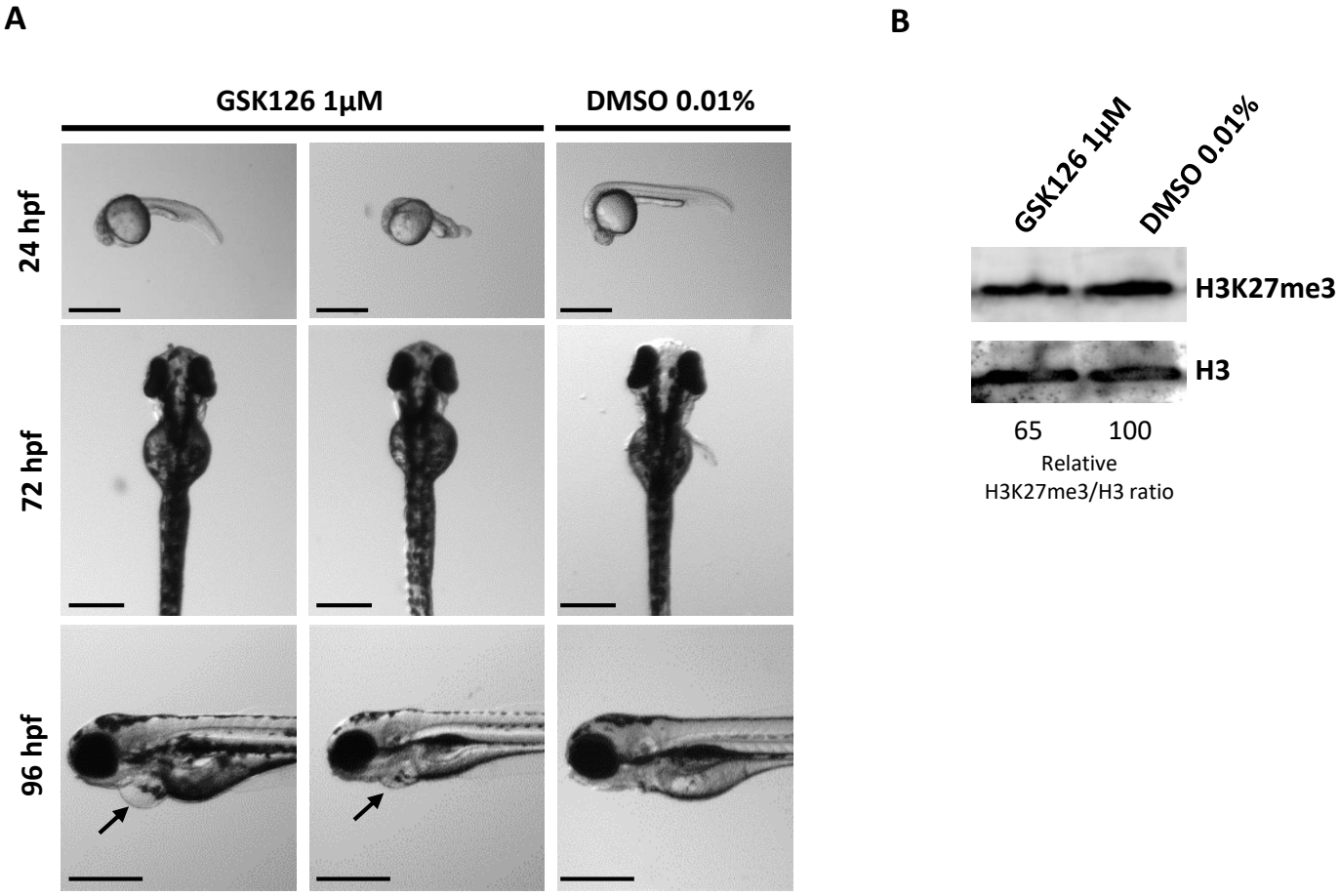

Dupret et al. – Additional Figure S5

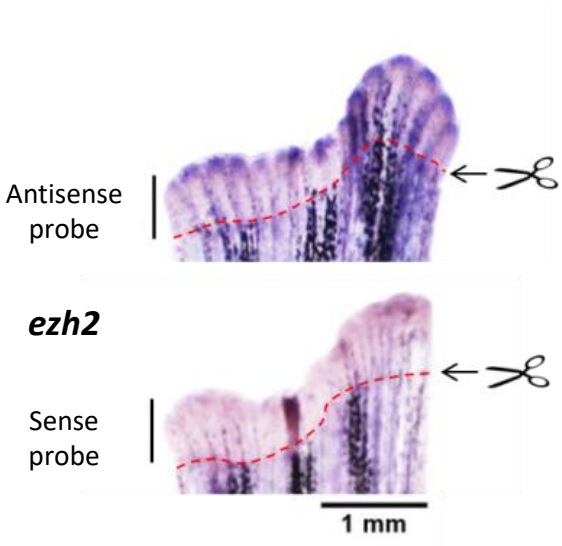

Dupret et al. – Additional Figure S6